5-23-66
AI
10 Copies

[redacted]

MASTER

NAA-SR-6320
VOLUME II OF VI
(TRW REPORT No. ER-6041)
AEC CATEGORY C-92B, M-3679 (43rd EDITION)
MERCURY RANKINE PROGRAM (SNAP 2) TOPICAL REPORT No. 28

MERCURY RANKINE PROGRAM (SNAP 2)

DEVELOPMENT OF LIQUID-MERCURY-LUBRICATED BEARINGS

VOLUME II

PLAIN BEARING EXPERIMENTAL RESULTS

(TITLE UNCLASSIFIED)

AEC RESEARCH AND DEVELOPMENT REPORT

PREPARED UNDER SUBCONTRACT N843 FS-101221
FOR

ATOMICS INTERNATIONAL
A Division of North American Aviation Inc.

TRW EQUIPMENT LABORATORIES
A DIVISION OF TRW INC. • CLEVELAND, OHIO 44117

MASTER

[redacted]

DISCLAIMER

Printed in USA Charge $1.30. Available from the

U. S. Atomic Energy Commission
Division of Technical Information Extension,
P. O. Box 62
Oak Ridge, Tennessee.

Please direct to the same address inquiries covering the procurement of other classified AEC reports.

NAA-SR-6320
VOLUME II OF VI
TRW REPORT No. ER-6041
AEC CATEGORY C-92B, M-3679 (43rd EDITION)
MERCURY RANKINE PROGRAM (SNAP 2) TOPICAL REPORT No. 28

MERCURY RANKINE PROGRAM (SNAP 2)

DEVELOPMENT OF LIQUID-MERCURY-LUBRICATED BEARINGS

VOLUME II

PLAIN BEARING EXPERIMENTAL RESULTS

(TITLE UNCLASSIFIED)

By

OTTO DECKER

PREPARED UNDER SUBCONTRACT N843 FS-101221
FOR

ATOMICS INTERNATIONAL
A Division of North American Aviation Inc.

TRW EQUIPMENT LABORATORIES
A DIVISION OF TRW INC. • CLEVELAND, OHIO 44117

CONTRACT: AT(II-I)-GEN-8
ISSUED:

DISTRIBUTION LIST

SYSTEMS FOR NUCLEAR AUXILIARY POWER (SNAP)
REACTOR SNAP PROGRAM
M-3679 (43rd Ed.)

No. of Copies		No. of Copies	
1	AEC Patent Office	1	Johns Hopkins University (APL)
6	Aerojet-General Corporation (NASA)	1	Lockheed-Georgia Company
1	Aerojet-General Corporation, Sacramento	1	Los Alamos Scientific Laboratory
1	Aerojet-General Nucleonics	1	Minnesota Mining and Manufacturing Company
1	Aerojet-General Nucleonics (NASA)		
2	Aeronautical Systems Division	1	Monsanto Research Corporation
1	Aerospace Corporation	1	Mound Laboratory
1	Air Force Foreign Technology Division	1	NASA Ames Research Center
1	Air Force Headquarters	2	NASA Goddard Space Flight Center
1	Air Force Surgeon General	7	NASA Lewis Research Center
1	Air Force Technical Applications Center	1	NASA Manned Spacecraft Center
3	Air Force Weapons Laboratory	3	NASA Marshall Space Flight Center
1	Air University Library	3	NASA Scientific and Technical Information Facility
1	AiResearch Manufacturing Company, Phoenix	2	National Aeronautics and Space Administration, Washington
1	Allison Division - GMC	4	National Reactor Testing Station (PPCO)
1	Argonne National Laboratory	1	Naval Air Development Center
1	Army Ballistic Research Laboratories	1	Naval Radiological Defense Laboratory
1	Army Director of Transportation	2	Naval Research Laboratory
1	Aro, Inc.	1	Navy Marine Engineering Laboratory
2	Atomic Energy Commission, Washington	1	New York Operations Office
66	Atomics International	1	Nuclear Weapons Training Center Pacific
1	Battelle Memorial Institute		
2	Battelle-Northwest	1	Oak Ridge Operations Office
1	Bendix Corporation (NASA)	2	Office of Naval Research
1	Brookhaven National Laboratory	1	Office of the Chief of Engineers
2	Bureau of Naval Weapons	3	Office of the Chief of Naval Operations
2	Bureau of Ships	2	Office of the Chief of Naval Operations (OP-03EG)
1	California Patent Group		
2	Canoga Park Area Office	1	Pratt and Whitney Aircraft Division (NASA)
1	Central Intelligence Agency		
1	Chicago Patent Group	1	Radio Corporation of America
1	Director of Defense Research and Engineering (OAP)	1	Rand Corporation
		1	Sandia Corporation
1	Douglas Aircraft Company, Inc. Newport Beach	8	Union Carbine Corporation (ORNL)
1	Du Pont Company, Aiken	1	United Nuclear Corporation (NDA)
1	Du Pont Company, Wilmington	1	University of California, Livermore
1	Electro-Optical Systems, Inc.	1	Westinghouse Electric Corporation, Lima
1	General Atomic Division		
1	General Dynamics/Convair (AF)	1	Westinghouse Electric Corporation, Lima (AF)
1	General Dynamics/Fort Worth		
1	General Electric Company, Cincinnati	1	Westinghouse Electric Corporation (NASA)
2	General Electric Company (FPD)		
1	General Electric Company (MSVD)	1	Westinghouse Electric Corporation (WAL)
2	General Electric Company, San Jose		
1	Hughes Research Laboratories	2	White Sands Missile Range
1	Institute for Defense Analyses	10	Division of Technical Information Extension
2	Jet Propulsion Laboratory		
		9	TRW Inc.

FOREWORD

This Development of Liquid-Mercury-Lubricated Bearings Topical Report defines the analytical and experimental results obtained with fluid film bearings lubricated by liquid mercury. This report includes the design approach, analytical techniques, procedures, test results, and experimental activity performed by TRW Inc. as a facet of the Mercury Rankine Power Conversion Program during the period of January 1961 through June 1963.

This report consists of the following six volumes:

Volume I	Analytical Design Approach and Status of Bearing Systems (With Appendixes)
Volume II	Plain Bearing Experimental Results
Volume III	Tilting-Pad Bearing Experimental Results
Volume IV	Three-Sector Bearing Experimental Results
Volume V	Three-Pad Bearing Experimental Results
Volume VI	Spiral-Groove Thrust Bearing Experimental Results

For convenience of the reader, citations of reference works are the same in each volume; e. g., Reference 6 cited in Volume I and Reference 6 cited in Volume II are the same publication.

Volume I contains the Nomenclature and the References on the study. All other Appendixes are also included in Volume I.

ABSTRACT

The performance characteristics of the plain (axial groove) journal bearings evaluated during this report period is presented in this volume. The influence of turbulent or superlaminar flow conditions in the clearance space on major parameters are established. Laminar flow equations for load capacity and power loss are modified by Reynolds number terms to account for the flow conditions in the clearance space although the plain journal bearing meets many of the turboalternator requirements. Its inherent instability, susceptibility to cavitation-erosion damage, and sensitivity to load direction prevents its further development for application in the long term CRU V.

TABLE OF CONTENTS

Section		Page
I.	INTRODUCTION - SUMMARY	9
II.	PLAIN BEARING	10
	A. Load Carrying Capacity	10
	B. Fluid Film Stiffness	20
	C. Attitude Angle (Ø)	22
	D. Stability	22
	E. Power Loss	30
	F. Flow	39
	G. Influence of Rotating Loads	46
	H. Damping Characteristics	51
	I. Film Continuity	56
III.	CONCLUSIONS	57

LIST OF ILLUSTRATIONS

Figure No.		Page
1	Typical Journal Bearing Geometries	11
2	Plain Axial Groove Bearing	12
3	Generalized Laminar and Turbulent Performance Characteristics of Plain Journal Bearing	13
4	Load Carrying Capacity vs Eccentricity Ratio	15
5	Imposed Unidirectional Internal Load as a Function of Supply Pressure for a Plain Journal Bearing	16
6	Experimental Results Compared to Predicted Performance for Plain Journal Bearing	17
7	Plain Bearing Turbulent Load Factor	19
8	Stability Characteristics of Plain Journal Bearing	21
9	Attitude Angle vs Eccentricity Ratio for Plain Journal Bearing	23
10	Attitude-Eccentricity Locus for a Plain Bearing	24
11	Whirl Characteristics	25
12	Predicted Radial Stiffness Characteristics for a Plain Journal Bearing	27
13	Predicted Half-Frequency Whirl Threshold for Plain Journal Bearings	28
14	Experimental and Theoretical Whirl Characteristics Showing Load to Suppress Half-Frequency Whirl for Turbulent Flow Plain Journal Bearing	29
15	Whirl Amplitude vs Rotor Speed for Plain Bearing	31
16	Whirl Amplitude vs Rotor Speed for a Plain Bearing with 30 lb/ Bearing Unbalance at 40,000 rpm	32
17	Power Loss Factor for Journal Bearings Operating in the Turbulent Regime	33

LIST OF ILLUSTRATIONS (Continued)

Figure No.		Page
18	Power Loss Factor vs Reynolds Number for Journal Bearings Operating in the Turbulent Regime	34
19	Experimental and Theoretical Turbulent Power Loss for 0.625-Inch Diameter, 0.312-Inch Length Plain Bearing	35
20	Experimental and Theoretical Power Loss for a Plain Journal Bearing Based on Smith and Fuller Data	37
21	Bearing Power Loss vs Rotor Speed for Two Plain Bearings and One Spiral Groove Thrust Bearing	38
22	Flow Factor for a Short Journal Bearing	40
23	Bearing Flow vs Shaft Speed for a Plain Journal Bearing	41
24	Experimental Flow Characteristics for a Plain Journal Bearing (Turbine End)	42
25	Flow Pressure Relationship for Plain Bearing with Downward Unidirectional Loads at 40,000 rpm	44
26	Load vs Flow at 30,000 rpm	45
27	Flow Calibration for a Plain Bearing with a Single Inlet at the Top Bearing - Turbine	47
28	Load vs Flow at 30,000 rpm Plain Bearing with Single Inlet at Top $\mathcal{L}$ (30 lb/Bearing Rotating Load at 40,000 rpm) (Turbine Bearing)	48
29	Flow Calibration for a Plain Bearing with Single Inlet at the Top - Test BETR 4B (Turbine Bearing)	49
30	Load vs Flow for a Plain Bearing with a Single Inlet at the Top at 20,000 rpm	50
31	Shaft Deflection vs Shaft Speed - Test BETR 4B	52
32	Synchronous Whirl Amplitude as a Function of Speed - BETR 4B Test Series	53

LIST OF ILLUSTRATIONS (Continued)

Figure No.		Page
33	Relative Phase Angle and Dynamic Deflection vs Rotor Speed . .	54
34	Relative Phase Angle and Dynamic Shaft Deflection vs Rotor Speed	59

LIST OF TABLES

Table No.		Page
1	Performance Summary for Five Journal Bearings	55

I. INTRODUCTION - SUMMARY

The plain or axial groove journal bearing was selected for development for the SNAP 2 turboalternator because of its geometric simplicity, its satisfactory load capacity, and its internal load mechanism. Earlier tests had been conducted with this type of bearing geometry, but insufficient instrumentation prevented adequate mapping of its performance characteristics. Reference (1) contains the prior data available on this type bearing.

A series of tests were conducted on a single plain bearing size. The major variables included bearing diametral clearance, type and magnitude of imposed load, speed and flow-pressure characteristics. The primary bearing characteristics investigated included load carrying capacity, attitude angle, fluid film stiffness, stability power loss, flow-pressure, damping and film continuity.

The plain journal bearing met many of the imposed CRU requirements. It was applied in several CRU models of the -I, -III, and -IVM configurations with varying success. Nevertheless, several major disadvantages prevented its incorporation in the later CRU designs, ie., CRU V. These included poor stability characteristics, poor life capability because of sensitivity to cavitation-erosion damage, unreliable flow characteristics, sensitivity to clearance changes, and high supply pressure requirements.

The simple geometry and predominantly hydrodynamic performance characteristics of the plain journal bearing permitted Reynolds number modifications to existing laminar flow equations which provided good representation of measured load capacity, attitude angle, and power loss.

II. PLAIN BEARING

A major part of the experimental program on plain journal bearings was conducted on bearings with a 0.625-inch diameter and 0.312-inch length. The bearing contains a single supply hole 0.060-inch diameter with a recessed supply pad approximately 1/8-inch long (in circumferential direction) by 1/4 inch wide (in axial direction). Figure 1 shows the plain bearing schematic (called axial groove) configuration. Figure 2 shows a photograph of the actual bearing used for component test after a series of startups.

The geometric variable between tests was diametral clearance, which was changed over a range from 0.0012 to 0.002 inch. For the 0.002-inch clearance bearing discussed here, three parametric test series were conducted. These tests designated BETR 4, 4A, and 4B established the influence of 0 lb, 30 lb, and 60 lb of rotating load per bearing. Data on different clearance plain bearings were previously reported in Reference 1.

A. LOAD CARRYING CAPACITY

Figure 3 shows the generalized performance parameters of such a plain journal bearing, i.e., 1/S vs ϵ . Before proceeding with correlation and analysis of experimental data, it is necessary to understand the reason for the different performance predicted for the turbulent case in Figure 3.

As discussed in the analysis section, Smith and Fuller's prediction assumes that the performance of a turbulent flow bearing approaches that of an infinitely long laminar bearing, i.e., flow in the axial direction is reduced, dependent of course upon the actual L/D ratio of the bearing under consideration. In this particular case, where L/D = 0.5 the correction for turbulence was assumed to be equivalent to operating a bearing having an L/D ratio equal to one. Making this modification results in the curve showing side flow leakage correction only.

To account for the high supply pressure, the bearing is assumed to approach a Sommerfeld bearing, where the negative pressures in the crown of the bearing become the mirror image of the positive pressures in the loaded side of the bearing. Including this modification and the end leakage correction results in the predicted curve, identified as Sommerfeld bearing.

Since the end leakage is large at low eccentricity ratios, the end flow assumption is optimistic. As the eccentricity ratio approaches 1.0, the assumption for turbulence agrees with the laminar flow bearing, since at ϵ = 1.0 the side leakage for the laminar bearing is zero. Figure 3 shows the Smith and Fuller turbulent curves approaching the laminar prediction as $\epsilon \rightarrow 1.0$.

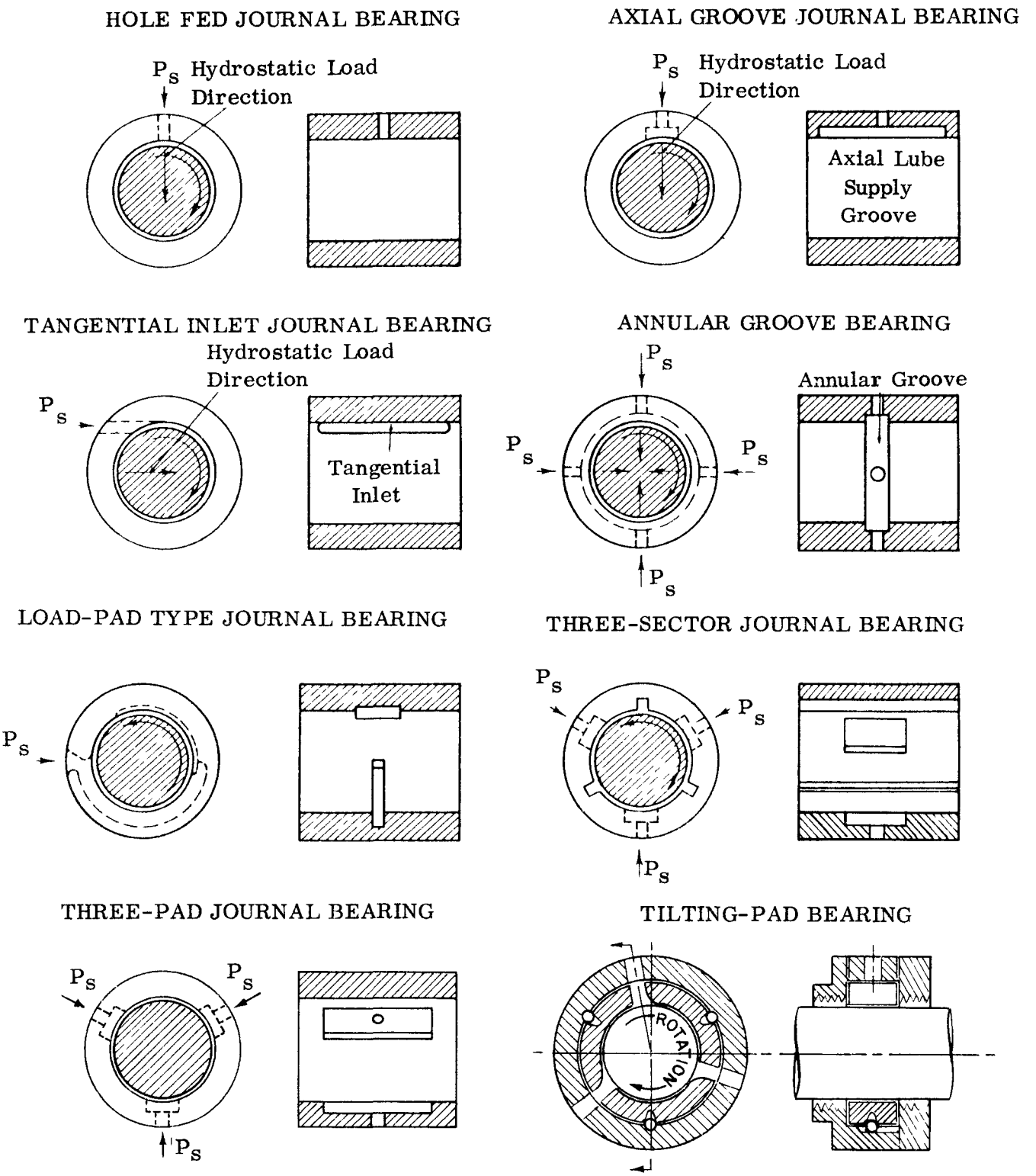

Figure 1. Typical Journal Bearing Geometries

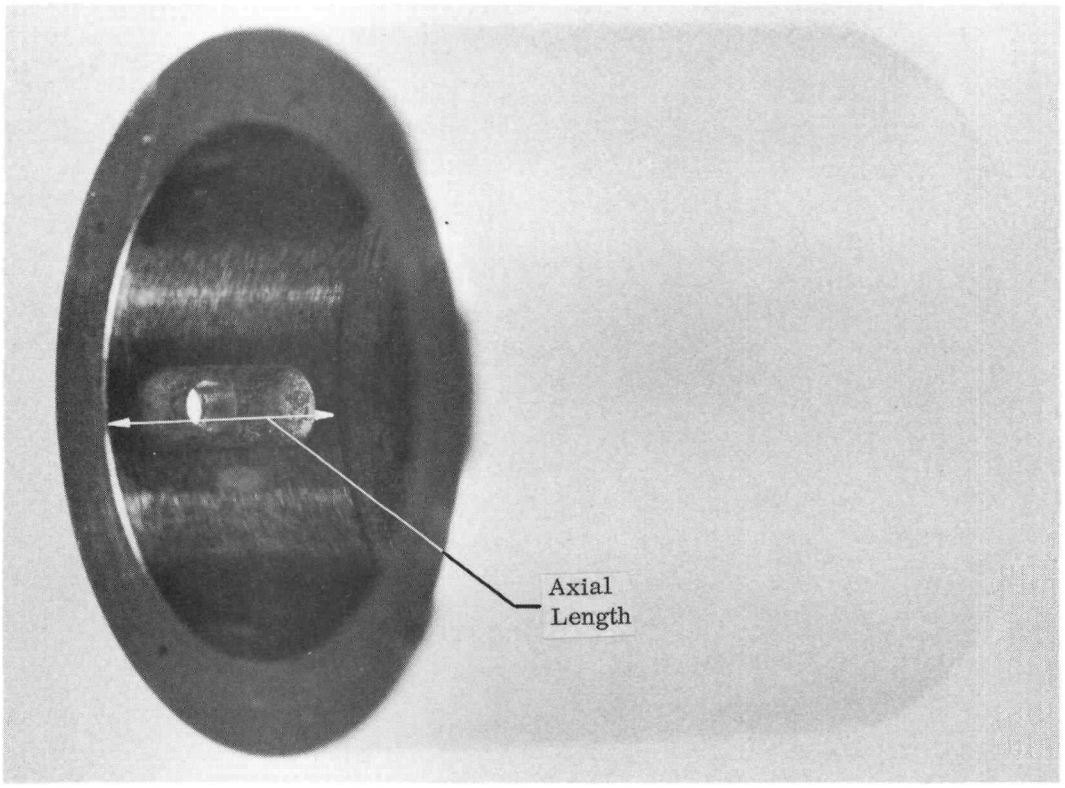

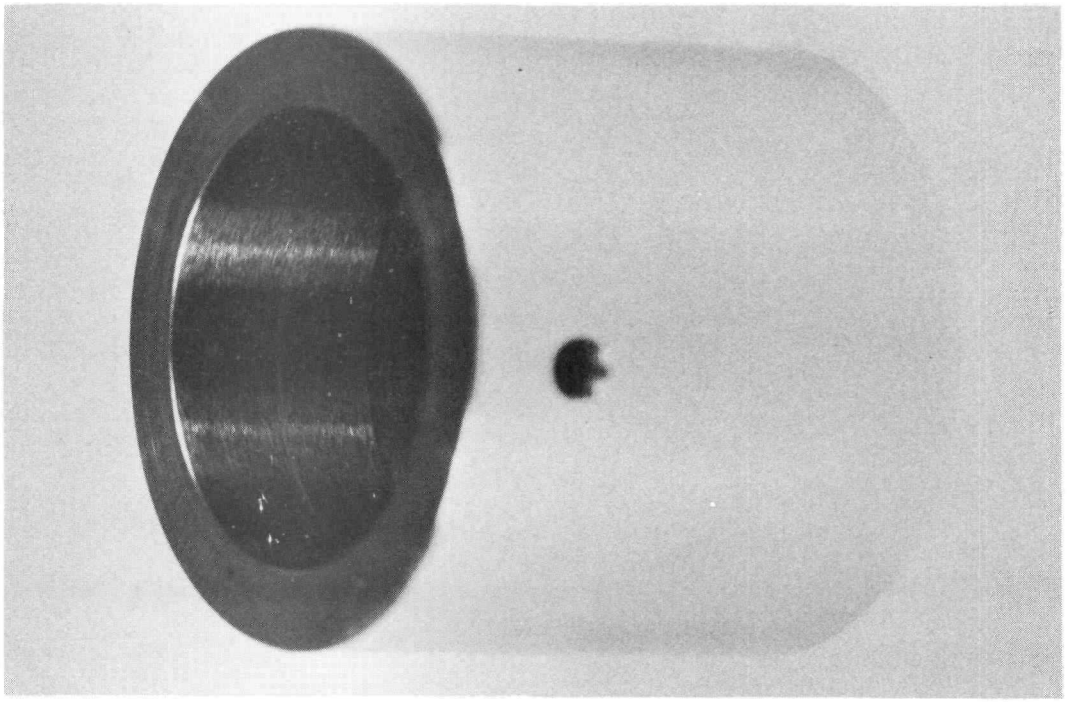

Figure 2. Plain Axial Groove Bearing

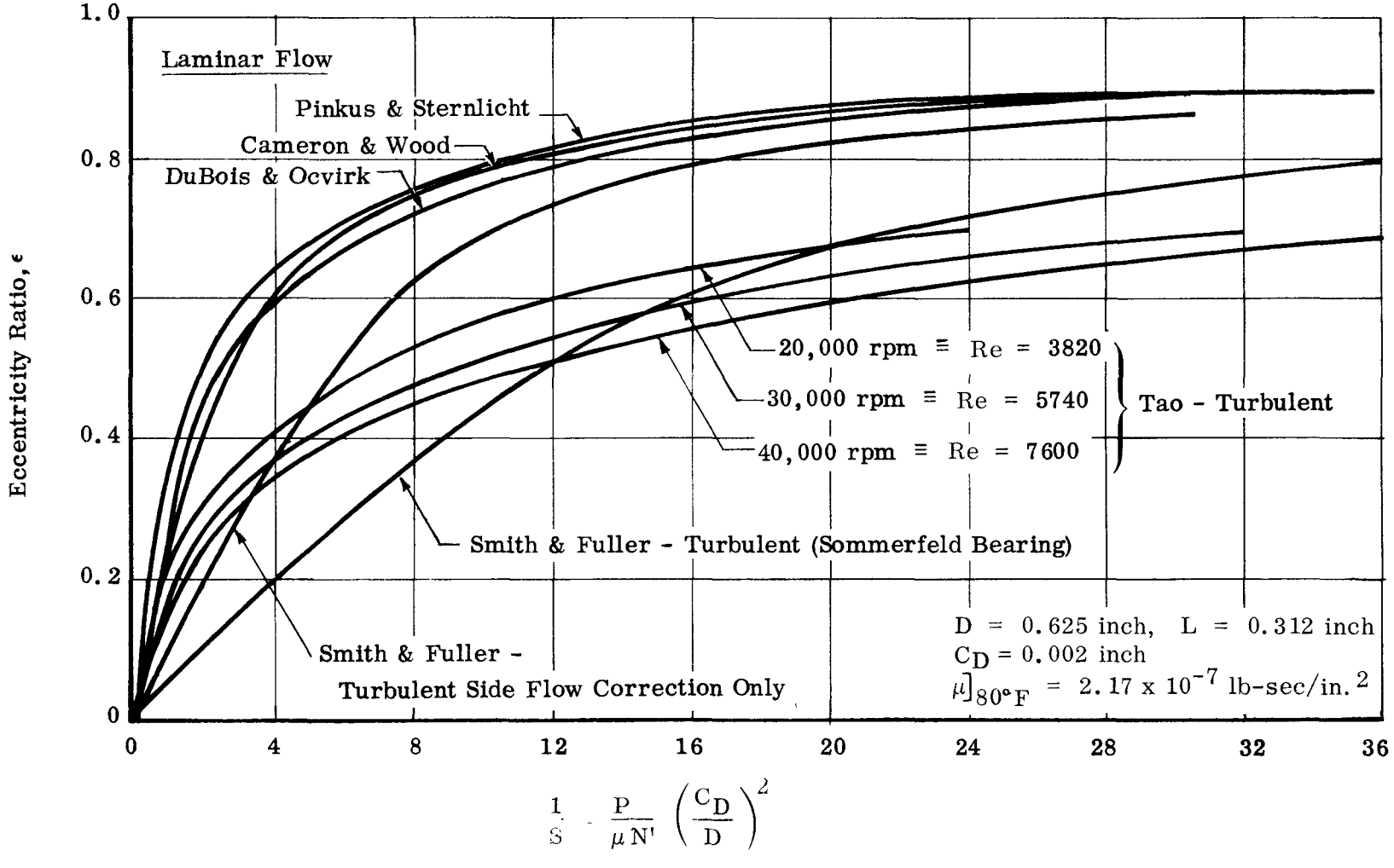

Figure 3. Generalized Laminar and Turbulent Performance Characteristics of Plain Journal Bearing

However, Tao (who assumes the pressure variation in the circumferential direction due to the convergent and divergent wedge to be negligible as compared to that in the axial direction) corrects his theory for Reynolds number and, consequently, derives a modified Sommerfeld number which contains Reynolds number for the turbulent case. Hence, at low turbulence his predicted curves are close to the laminar case, but as the turbulence increases they move further away from the laminar case. Since Reynolds number is included, each speed (so long as flow is turbulent) has its discrete, generalized performance curve, and, even at large values of eccentricity ratio, the turbulent and laminar predictions cannot approach each other. However, this assumes a Reynolds number based on mean film thickness.

As generally predicted, the actual turbulent load-carrying capacity is greater than the laminar prediction for each bearing tested. Figure 4 shows load-carrying capacity for the plain bearing. The actual load consists of the applied unidirectional load plus the internal load due to the high supply pressure. Performance of this type bearing is relatively unaffected by supply pressure. The slight effect of pressure is to increase the load capacity with increasing pressure as a result of establishing a pressure region in the unloaded side of the bearing that is negative with respect to that generated in the loaded side. Figure 5 shows the unidirectional load as a result of supply pressure.

For the hydrodynamic bearings, the increased load capacity due to turbulence is a definite advantage since it permits use of smaller bearings which, in turn, minimize the power loss. However, the stronger bearing operates close to the concentric position, i.e., $\epsilon \approx 0$, and results in unfavorable attitude angles and lowers the half-frequency whirl thresholds.

Both hydrodynamic and hybrid (both hydrostatic and hydrodynamic) bearings indicate a definite Reynolds number effect as shown in Figure 6, i.e., the generalized performance showing Sommerfeld number versus eccentricity ratio results in a distinctly different curve for each Reynolds number. For a laminar flow hydrodynamic bearing, just one curve explains Sommerfeld number as a function of eccentricity ratio.

Figure 4 indicates that the Smith and Fuller approach of merely including the turbulent end leakage correction provides good correlation. Including a factor of two i.e., approaching the full Sommerfeld bearing, in addition to the end leakage correction and Tao's predictions are too optimistic as indicated in Figure 6.

Figure 6 shows both experimental and predicted performance of a plain journal bearing. Variation from predicted laminar performance is greatest at smaller eccentricity ratios, i.e., $\epsilon < 0.5$. As $\epsilon \rightarrow 1.0$ turbulent load capacity approaches that predicted by laminar theory. This confirms the trends established by Smith and Fuller who indicated that laminar flow is reestablished at larger eccentricities in the loaded portion of the bearing. As a result, any solution for turbulent flow bearings which includes a Reynolds number or some other constant - such as Prandtl's mixing length constant which, as

Flow - Variable
Bearing Type - Plain
m = 0.0032 L/D = 0.5

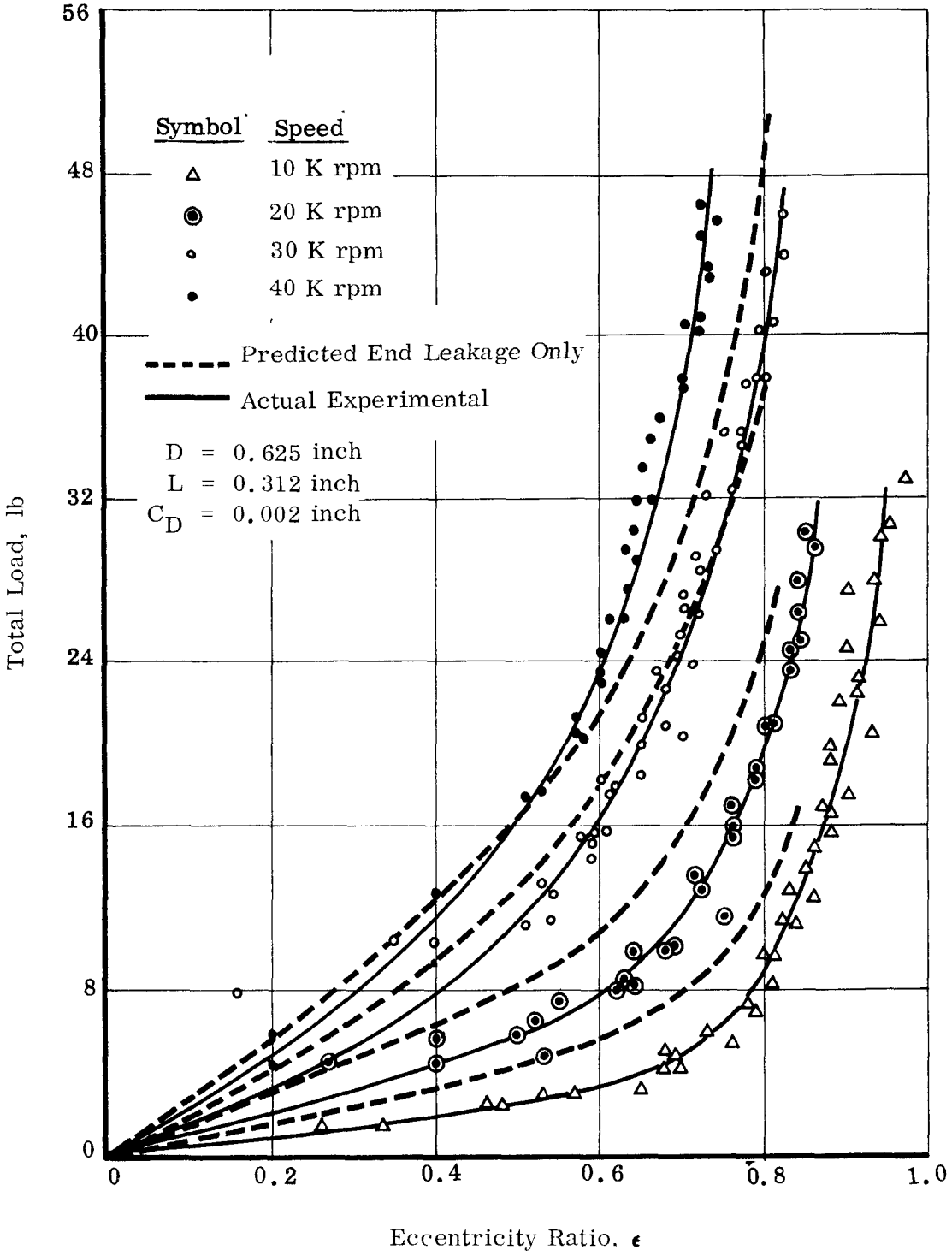

Figure 4. ad Carrying Capacity vs Eccentricity Ratio

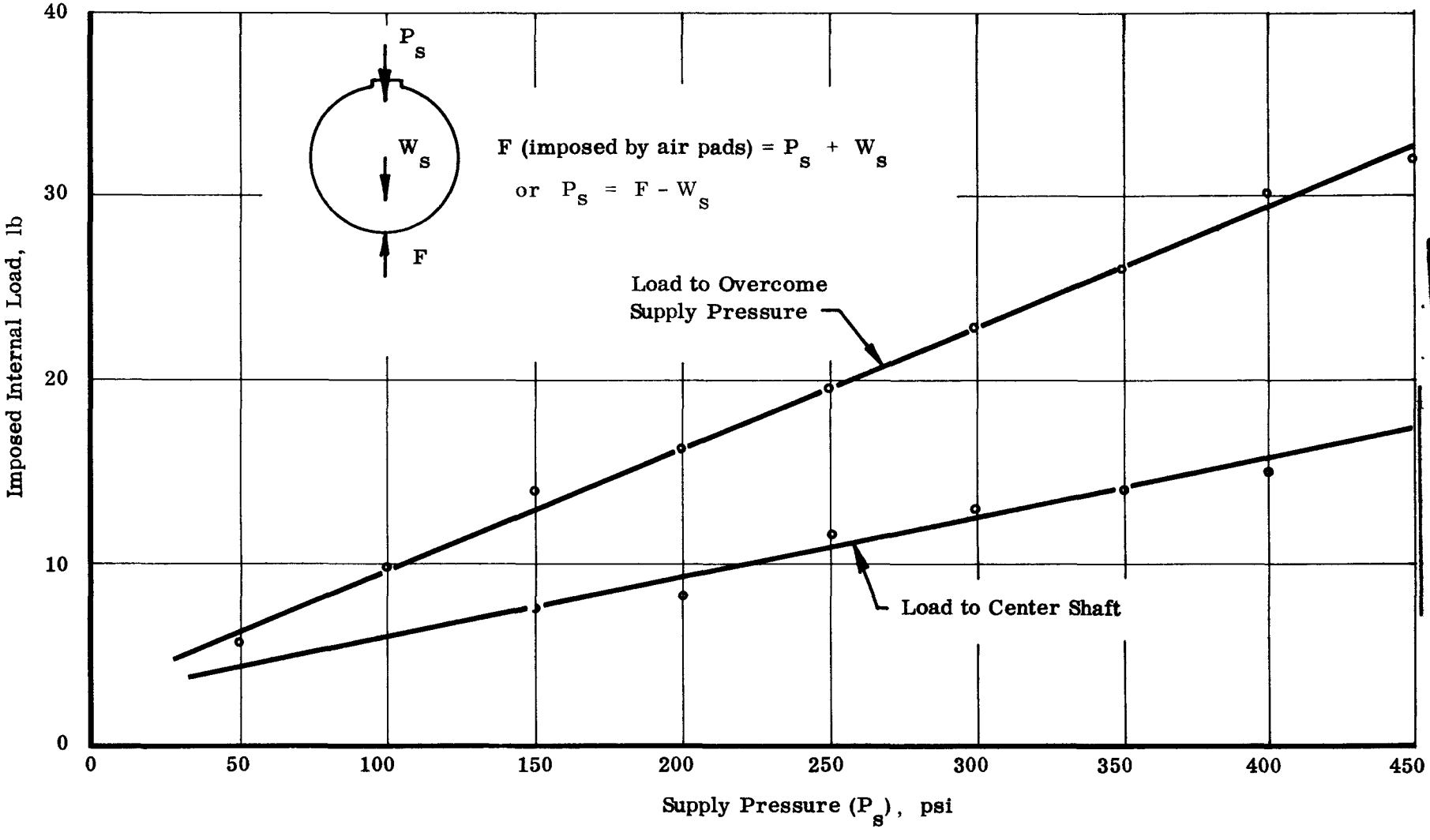

Figure 5. Imposed Unidirectional Internal Load as a Function of Supply Pressure for a Plain Journal Bearing

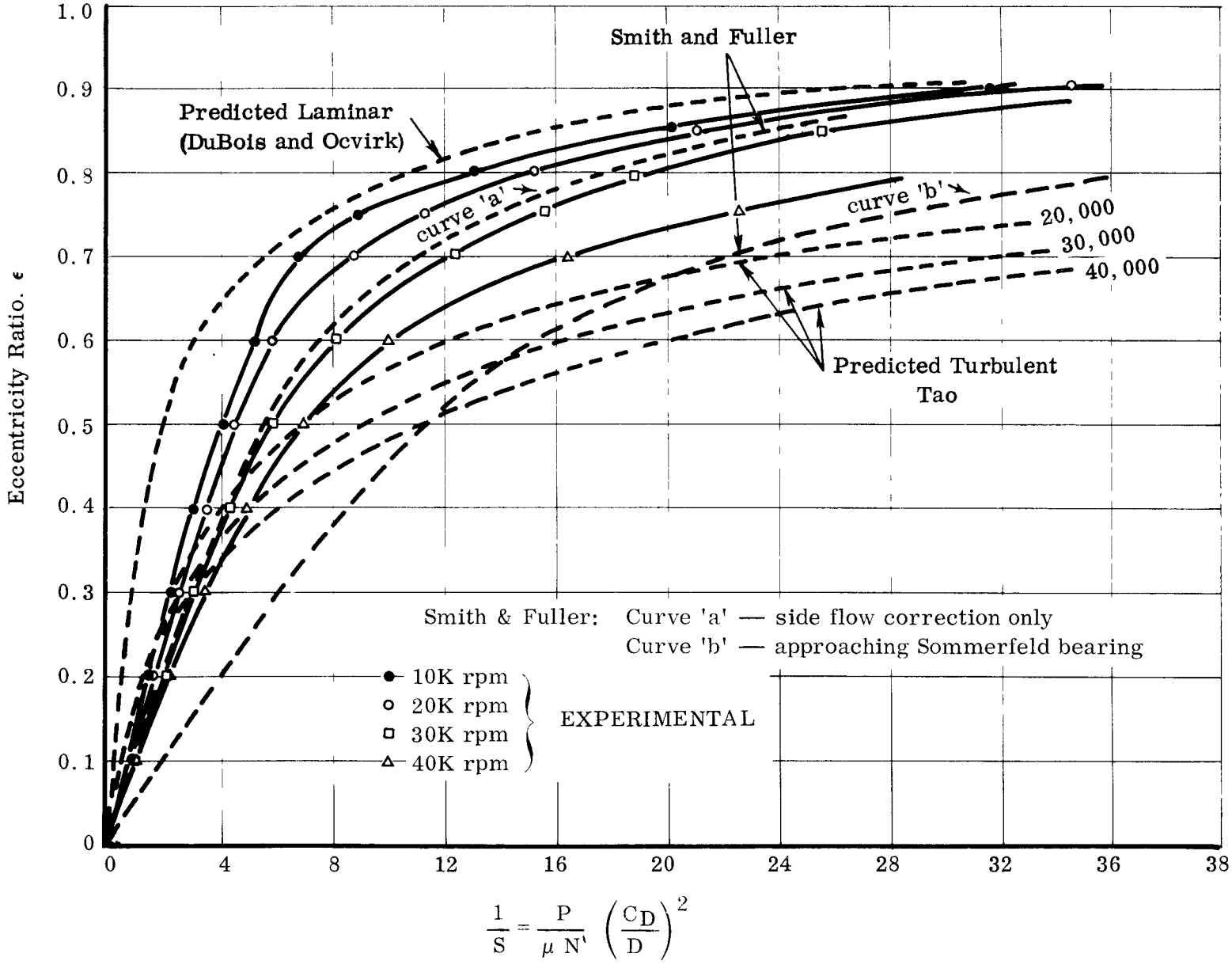

Figure 6. Experimental Results Compared to Predicted Performance for Plain Journal Bearing

indicated previously, some investigators use to consider the effects of turbulence, must reflect a Reynolds number which is some function of shaft position and not merely an average value. The Reynolds number that exists at the point of minimum film thickness (or the film thickness upon which the load capacity is based, in the case of self-aligning types) has been used to establish an empirical equation for turbulent load capacity. Figure 7 is a replot of the data between $0.2 < \epsilon < 0.8$ from Figure 4.. Data from the 10,000; 20,000; 30,000; and 40,000 speed lines are compared to the laminar prediction. The ratio when plotted against the Reynolds number at the point of minimum film thickness falls in the general vicinity of the straight line whose equation is

$$K = W_T/W_L = 0.0301\ Re_{h_o}^{0.553} \qquad \ldots 1$$

Unit pressures from 100 to 500 psi are possible for turbulent flow, liquid-mercury-lubricated hydrodynamic bearings. In comparing these experimental characteristics to the theoretical values, the following observations may be made:

1) At all eccentricity ratios evaluated, load capacity is somewhat less than predicted by the Smith and Fuller method of reduced end leakage and high ambient pressure correction (curve b). When assuming that the high ambient pressure only provides an internal load and not a Sommerfeld bearing (curve a), Smith and Fuller's prediction based on end leakage correction agrees better. However, only at $R \approx 4,500$ is there good agreement. Agreement is good when comparing load capacity directly, as indicated in Figure 4.

2) The variation of 1/S with eccentricity ratio at values of ϵ is influenced by Reynolds number similarly to that predicted by Tao's modified Sommerfeld number.

3) The actual load capacity is smaller than predicted by Tao for values of $\epsilon > 0.5$, assuming the Reynolds number based on the mean film thickness. For a Reynolds number correction based on minimum film thickness the agreement would be better. However, this is to be expected, since at greater eccentricity ratios, the flow is no longer turbulent throughout the entire bearing, but tends to become laminar in the loaded portion of the bearing, i.e., where clearance is small.

4) At values of $\epsilon > 0.5$, flow remains turbulent throughout the entire clearance space. As shown by the flow data and tests in a transparent flow rig where visual observations of flow were possible, the majority of the flow is circumferential, although some is axial. Under those conditions, the performance of the bearing would approach that predicted by Smith and Fuller and would not agree very well with Tao who neglects the pressure variation in the circumferential direction. That the load capacity is lower than that predicted by Smith and Fuller is probably due to the assumption of greatly reduced axial flow and the factor 2 in the load capacity equation for high ambient pressure. When the assumption for the higher ambient pressure was not included, the method of merely modifying end leakage would result in reasonably close correlation with actually measured load capacity.

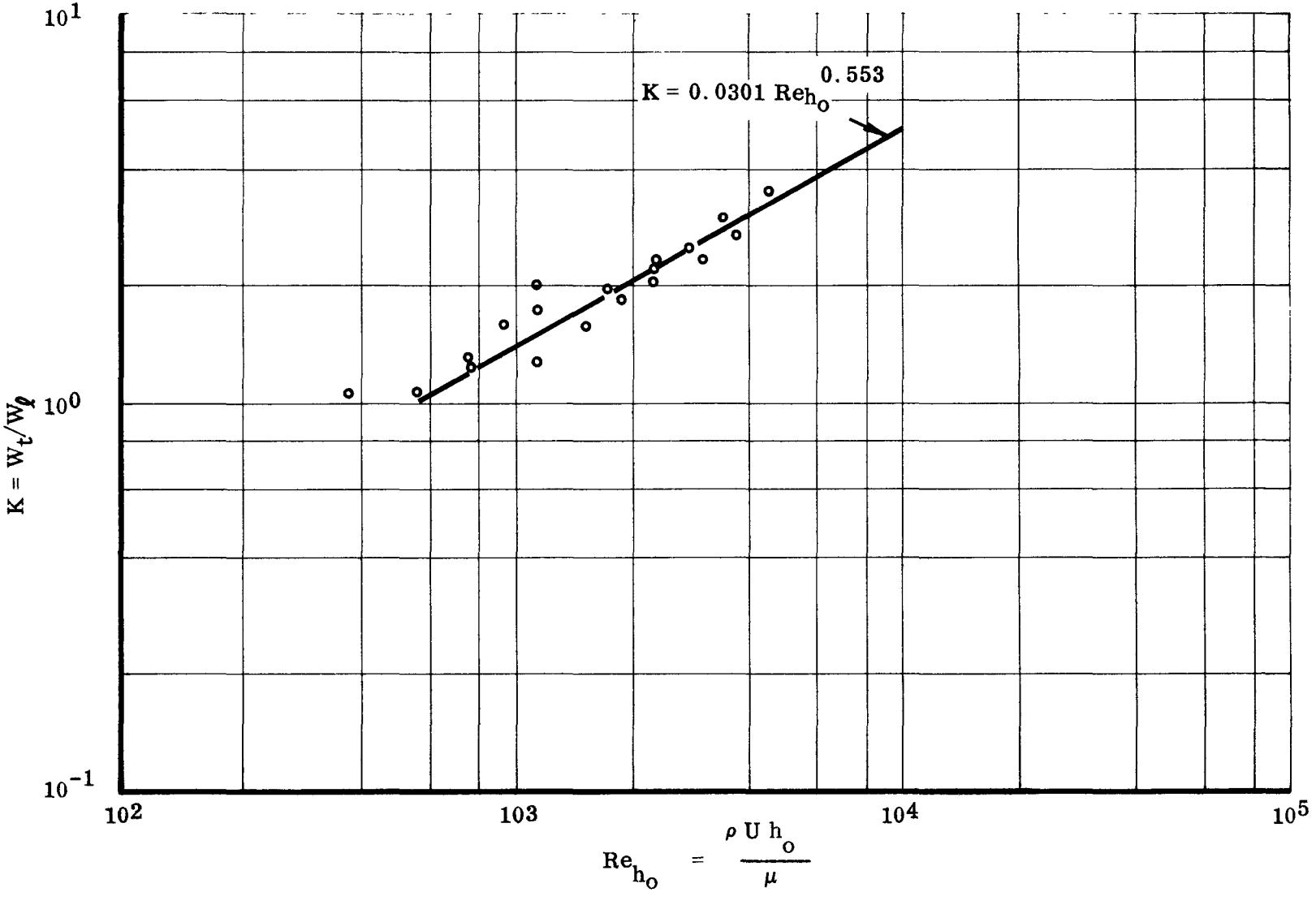

Figure 7. Plain Bearing Turbulent Load Factor

5) At speeds of 10,000; 20,000; and 30,000 rpm and at large eccentricity ratios, the load capacity appears to approach the laminar prediction. Smith and Fuller pointed out in their experiments that even for Reynolds numbers equal to five times the critical Reynolds number, the bearing performance could be predicted satisfactorily on the basis of laminar flow. At 20,000 rpm for this particular bearing, this critical Reynolds ratio is approximately 5.0. Should laminar flow then exist at the point of minimum film thickness, performance is expected to approach the laminar case.

6) Flow pressure characteristics, discussed later, indicate the need for high inlet pressures to provide adequate lubricant to the bearings. In addition to creating ambient pressure (up to 400 psi) which complicates the analysis, considerable unidirectional loads are applied as a result of this high pressure pocket. The experimental results are compensated for this additional load applied to the shaft by calibrating the load required to overcome this internal force acting vertically downward. Under zero-gravity operation this internal, unidirectional load can be utilized to displace the shaft and to provide the necessary stability. It has been shown experimentally that the supply pressure can be utilized to suppress half-frequency whirl, once it is encountered, to the limit of pressure available. A later figure (Figure 8) which shows the load required to suppress whirl, indicates that both the load obtained by supply pressure and the load applied through external load-pads fall on the same line. This assures the accuracy of the calibration of supply pressure and the resultant internal applied load.

B. FLUID FILM STIFFNESS

The fluid film stiffness (dW/de) is greater than laminar theory predicts because of the improved load capacity with turbulent flow. This had advantages and disadvantages. When considering the relationship between bearing stiffness and rotor dynamics for power plants similar to SNAP, the bearing stiffness creates a problem. Generally, the fluid film stiffness is of the order of $K \approx 10^5$ lb/in. for bearings that are large enough to support the required loads and small enough to minimize power loss, i.e., keep Reynolds numbers low. This range of stiffness is not large enough to stay below, or small enough to stay above, the critical speed of the rotor-bearing combination. Consequently, for SNAP or test rig bearing-rotor combinations, at least the first mode critical speed is encountered in reaching the operating speed. For units with overhung masses, such as NaK pump rotors, the second mode must also be considered. The damping characteristics of mercury-lubricated bearings, discussed below, reduce the problem of passing through or operating close to these resonances.

The influence of bearing performance (stiffness and damping) on critical speed and rotor dynamics will be covered in a separate section.

m = 0.0032
L/D = 0.5
D = 0.625

Balanced Shaft	30 Lb/Brg Rotating Load At 40 KRPM	Method of Suppressing Whirl
✣	+	Suppressed By Supply Pressure Only With Shaft Supported (Zero-G)
○	●	Suppressed By Supply Pressure Only With Shaft Weight Acting
□	■	Suppressed By Unidirectional Load At Constant Supply Press. of 200 psi
△	▲	Suppressed By Unidirectional Load At Constant Supply Press. of 250 psi
▽	▼	Suppressed By Unidirectional Load At Constant Supply Press. of 300 psi

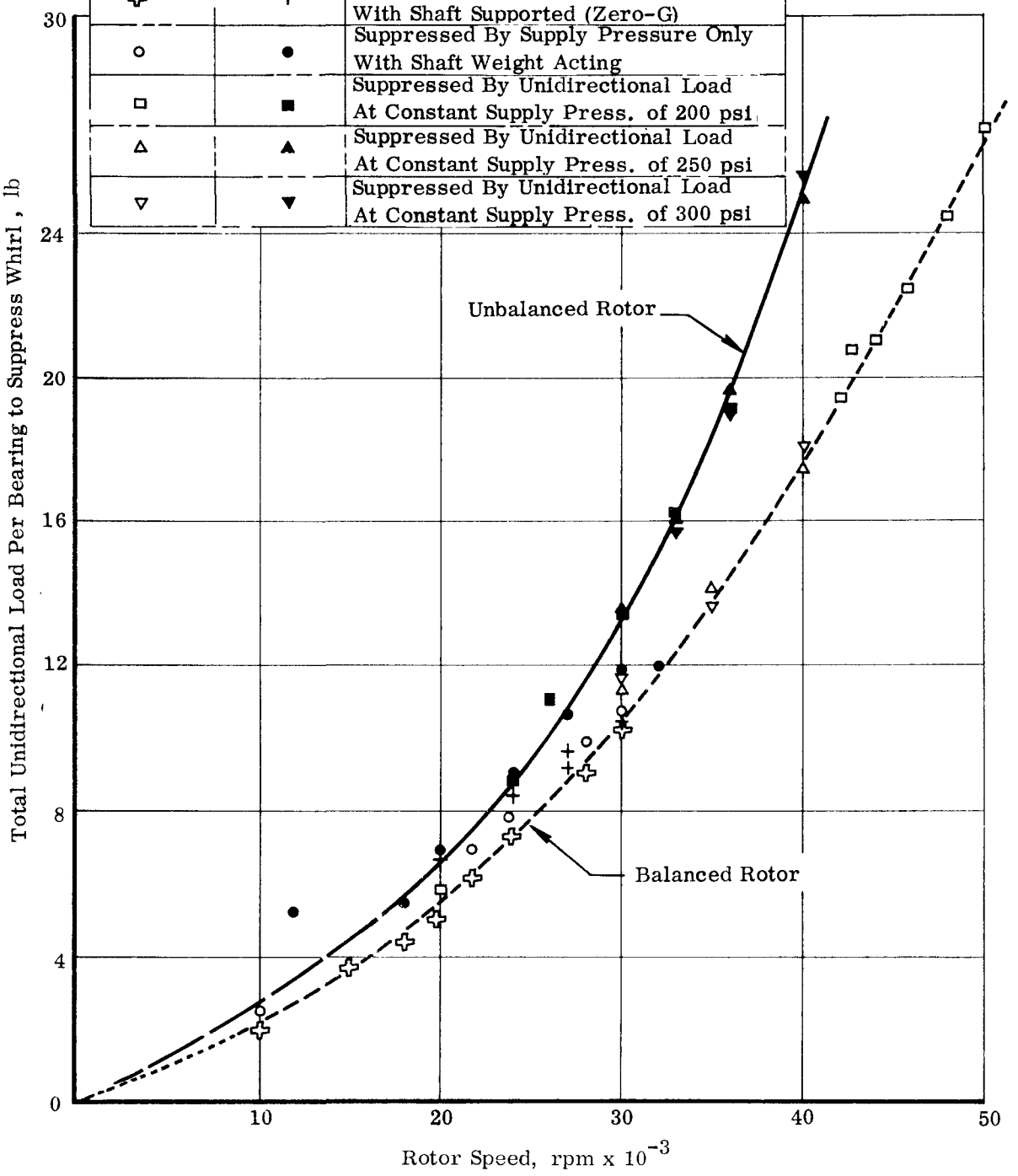

Figure 8. Stability Characteristics of Plain Journal Bearing

C. ATTITUDE ANGLE (Ø)

Figure 9 shows the attitude angle predicted by various investigators. Superimposed on Figure 9b is the mean of the experimental data obtained with the 0.002-inch plain bearing. Figure 10 shows the scatter of the actual data at speeds of 10,000; 20,000; 30,000; 35,000; and 40,000 rpm on a polar plot. These data were obtained, in conjunction with the load-deflection test discussed previously, by using two capacitance displacement probes located 90 degrees apart, i.e., one vertically, the other horizontally over the shaft. The experimental data show excellent agreement with the actual experimental points of Smith and Fuller.

1) As anticipated, the attitude angle is greater for the turbulent case than for the laminar. To eccentricity ratios of 0.65, the actual attitude angle is slightly greater for a given eccentricity ratio than that predicted for turbulent flow by the investigators referenced in this report. Smith and Fuller actually predict a locus (based on their analysis, but not supported by their results) which is approached by these experimental results. This indicates that the journal center moves further in the direction of rotation than predicted and will have a greater tendency toward instability (half-frequency whirl).

2) At values of $\epsilon > 0.65$, the measured angle is somewhat less than that predicted by analysis. This again is to be expected, since at these large eccentricities the minimum film thickness is so small that laminar flow is reestablished in the loaded portion of the film.

D. STABILITY

Two types of instability are of primary concern: (1) synchronous whirl (shaft orbiting in the bearing at rotational frequency) and (2) half-frequency or fractional frequency whirl (shaft orbiting in the bearing at one-half rotational frequency). Typical examples are presented in Figure 11. Synchronous whirl is of concern because the predominant load in space is a rotating load caused by mechanical and magnetic unbalance. The amplitude of this whirl component creates a problem if it assumes too large a percentage of the bearing clearance space. Hydrodynamic-type bearings, which have low stiffness at small eccentricity ratios and low speeds, have fairly large synchronous whirl amplitudes. Operation above the first mode critical speed has some advantage because the amplitude of the synchronous whirl component is fixed and will not grow rapidly as a function of speed squared.

The turbulent flow bearing generally has a lower half-frequency whirl threshold than the equivalent laminar flow bearing. The primary reason is that the resultant eccentricity ratio is smaller and the attitude angle larger in the turbulent flow bearing than in the laminar bearing for a given load. Figures 6 and 10 clearly demonstrate this. Operation of turbulent incompressible flow bearings with half-frequency whirl is

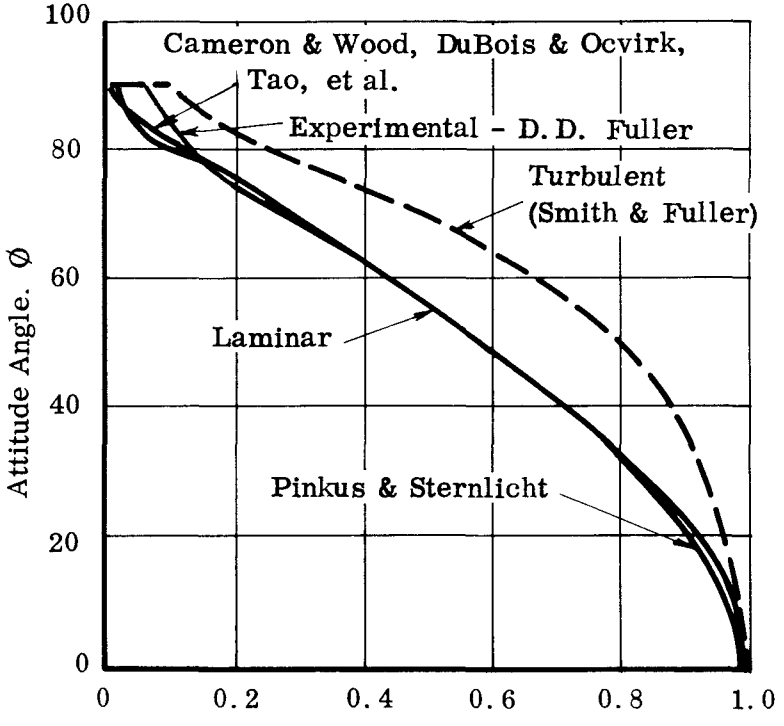

(a) Laminar Flow

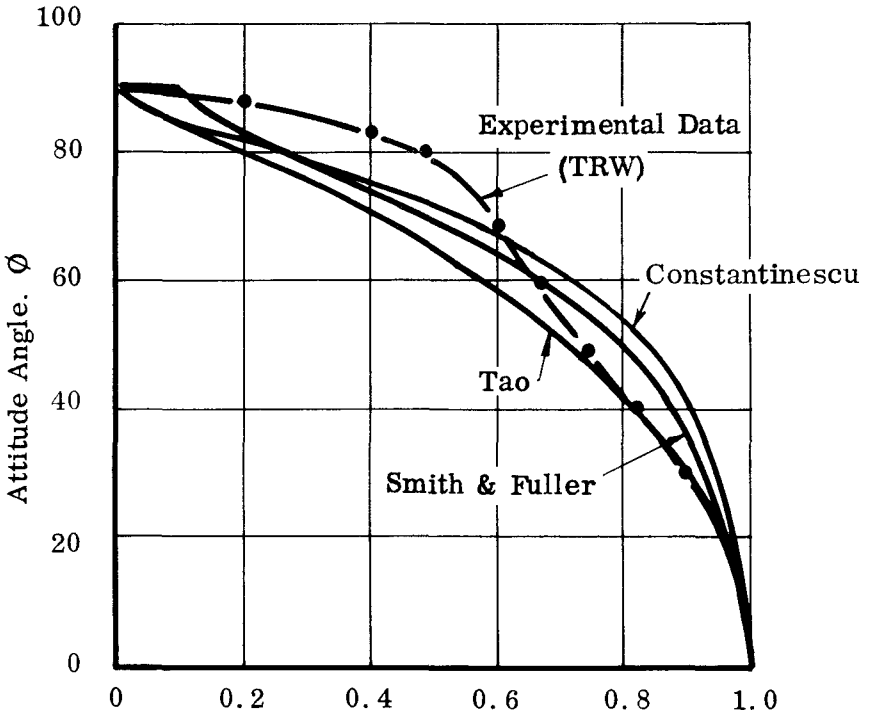

(b) Turbulent Flow

Figure 9. Attitude Angle vs Eccentricity Ratio for Plain Journal Bearing

(L D 0.5)

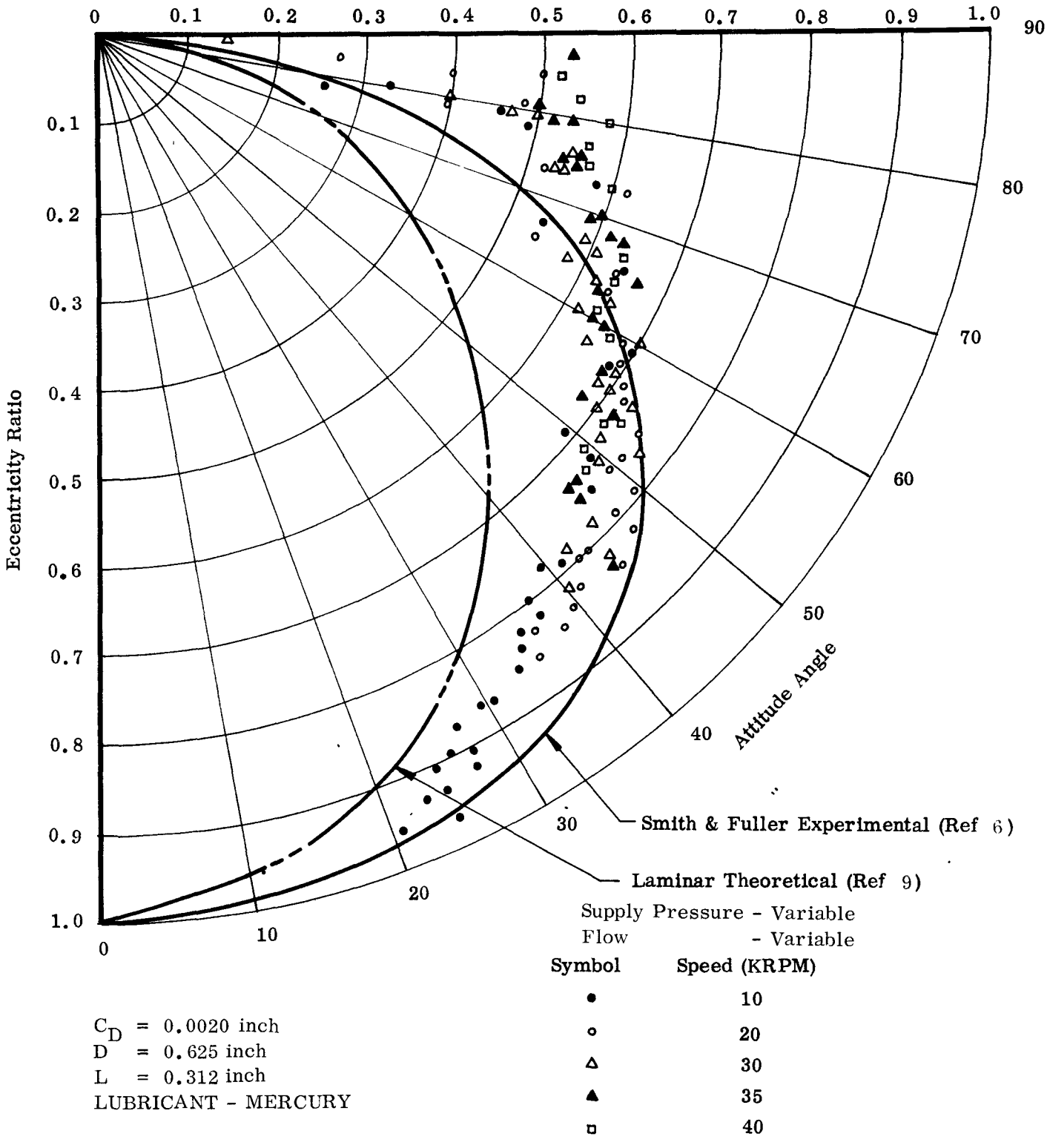

Figure 10. Attitude - Eccentricity Locus for a Plain Bearing

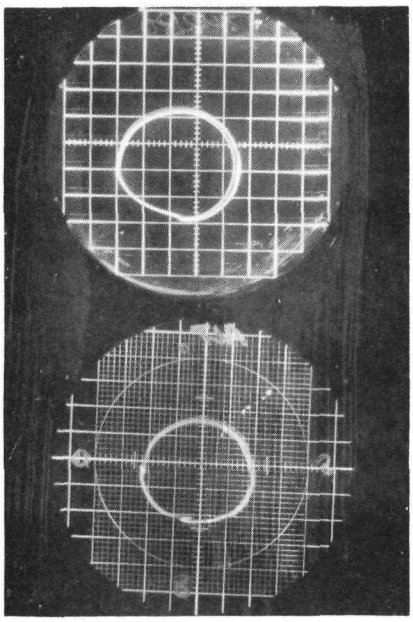

Locus in two separate planes N = 7,100 rpm with unbalanced rotor.

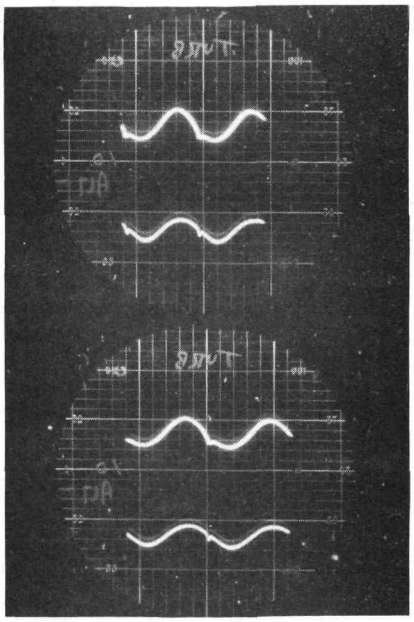

Individual amplitudes at 17,400 rpm (bottom) and 20,100 rpm (top) with unbalanced rotor.

(a) SYNCHRONOUS WHIRL

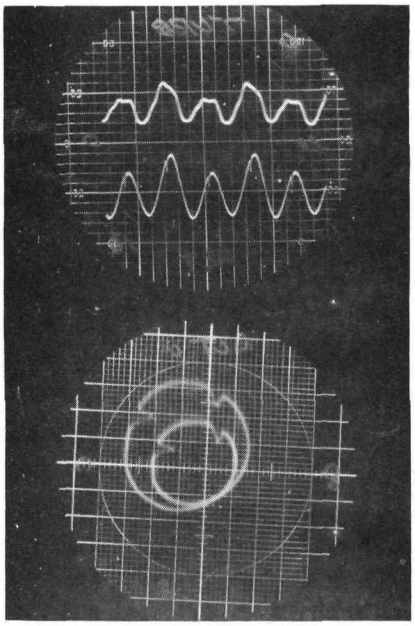

Threshold of half-frequency whirl with large synchronous whirl component N = 40,000 rpm.

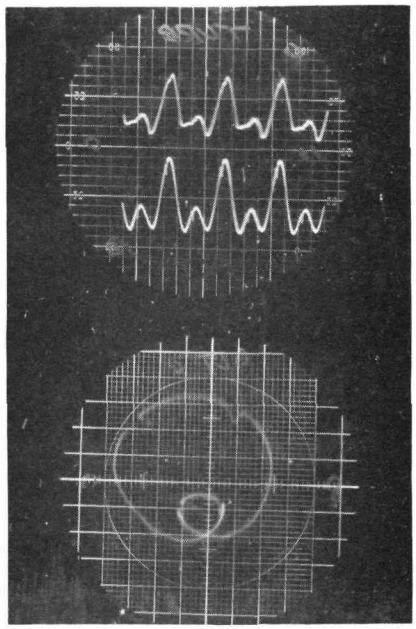

Half-frequency whirl component overcoming synchronous whirl component N = 30,000 rpm.

(b) HALF-FREQUENCY WHIRL

Figure 11. Whirl Characteristics

possible without destructive results, whereas this is not possible with compressible flow. Figure 8 is a plot of unidirectional load required to avoid half-frequency whirl for both a balanced and unbalanced rotor. The unbalanced rotor requires more unidirectional load to suppress half-frequency whirl. Half-frequency whirl was encountered as low as 10,000 rpm at simulated zero g. The data when extrapolated to zero indicates that this bearing type can be expected to have half-frequency instability at all speeds from 0 speed on, unless some form of unidirectional load is applied. Unfortunately the supply pressure could not be decreased sufficiently to investigate stability characteristics below a unidirectional load of 4 lb/bearing.

From the generalized curves of 1/S versus ϵ (Figure 6) and the attitude-eccentricity locus (Figure 9), the generalized plot of 1/S cos $\emptyset$ versus ϵ was obtained. The result, Figure 12, shows the turbulent prediction using both the Smith and Fuller approach and the Tao method. From the slope of Figure 12 and the procedure outlined in Section 3.3.5 the radial stiffness is obtained. The standard load-deflection curve combined with the attitude angle as a function of eccentricity ratio can also be used to establish the radial stiffness by establishing the slope at discreet points.

As the result of the turbulent flow characteristics; i.e., smaller eccentricity ratios, larger attitude angles, when compared with the laminar bearings; the analysis predicts a lower whirl threshold for the turbulent bearing. The crossover of Tao's and Smith and Fuller's curves at small eccentricity ratios (see Figure 12) also results in a crossover of predicted stability characteristics at equally small eccentricity ratios. Figure 13 was obtained by using the procedure discussed in Paragraph III-C-5 of Volume I. The Tao analysis predicts a more stable bearing than does the Smith and Fuller analysis because of the higher radial stiffness. When compared on the basis of load required to suppress the instability (obtained from the locus of points on Figure 13 and the corresponding load at that speed and eccentricity ratio from Figure 6), Tao's theory predicts a lower load to suppress whirl for all speeds up to 40,000 rpm. Figure 14 presents the load required to suppress whirl derived from the locus of the threshold points in Figure 13 and the corresponding loads obtained from Figure 6.

Figure 14 shows the excellent agreement between measured load to suppress half-frequency whirl and that predicted by Smith and Fuller's approach considering the turbulent end leakage correction only. No attempt was made to modify the end leakage correction established as a result of the experimental work of Smith and Fuller to assure agreement with the predictions. Tao's prediction performance is quite conservative but does show the influence of Reynolds number, which the experimental data have verified.

The most significant factor, however, is that regardless of which theory is selected as best suited to the special case, turbulent flow plain bearings are generally more unstable than their laminar counterparts.

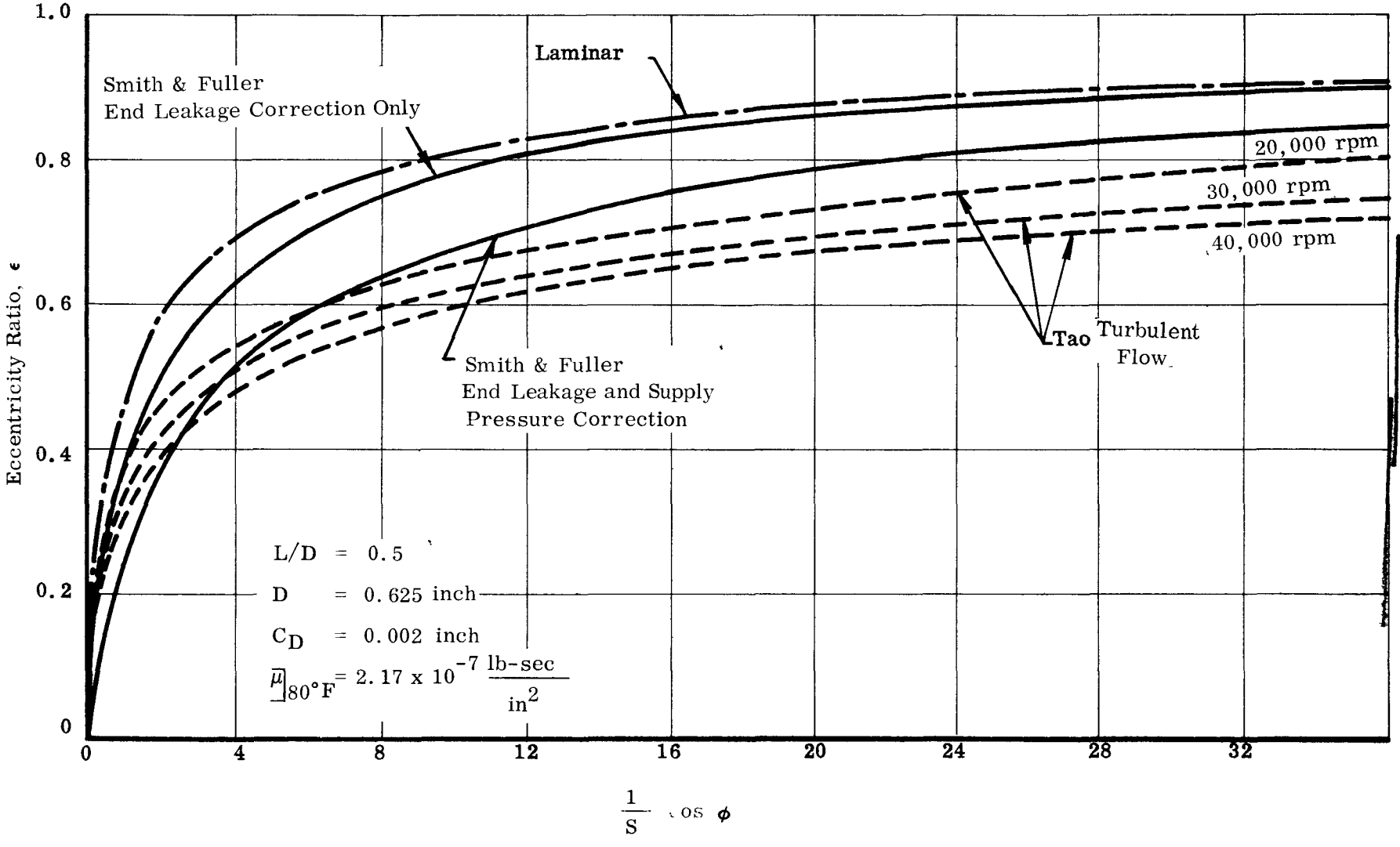

Figure 12. Predicted Radial Stiffness Characteristics for a Plain Journal Bearing

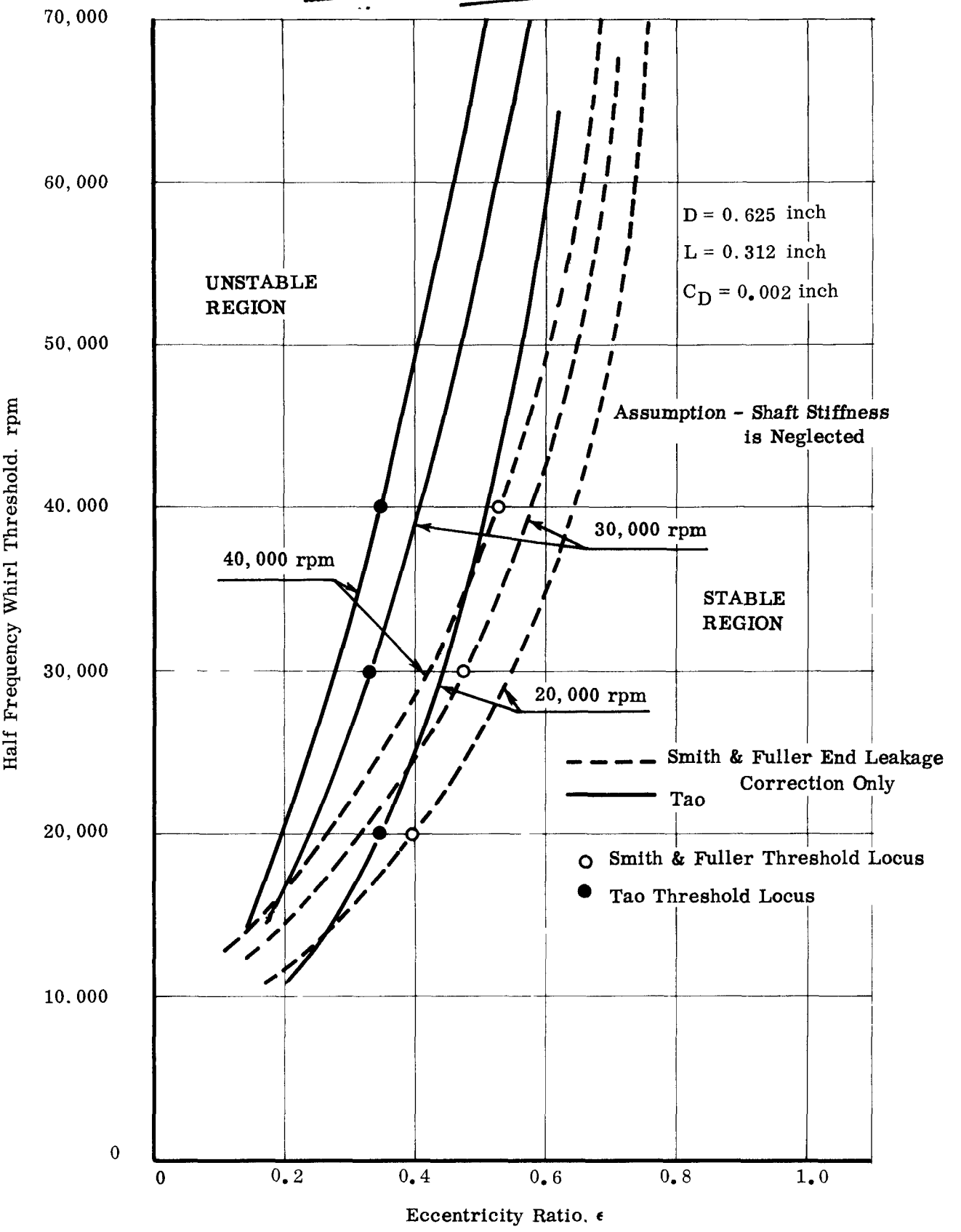

Figure 13. Predicted Half-Frequency Whirl Threshold for Plain Journal Bearings

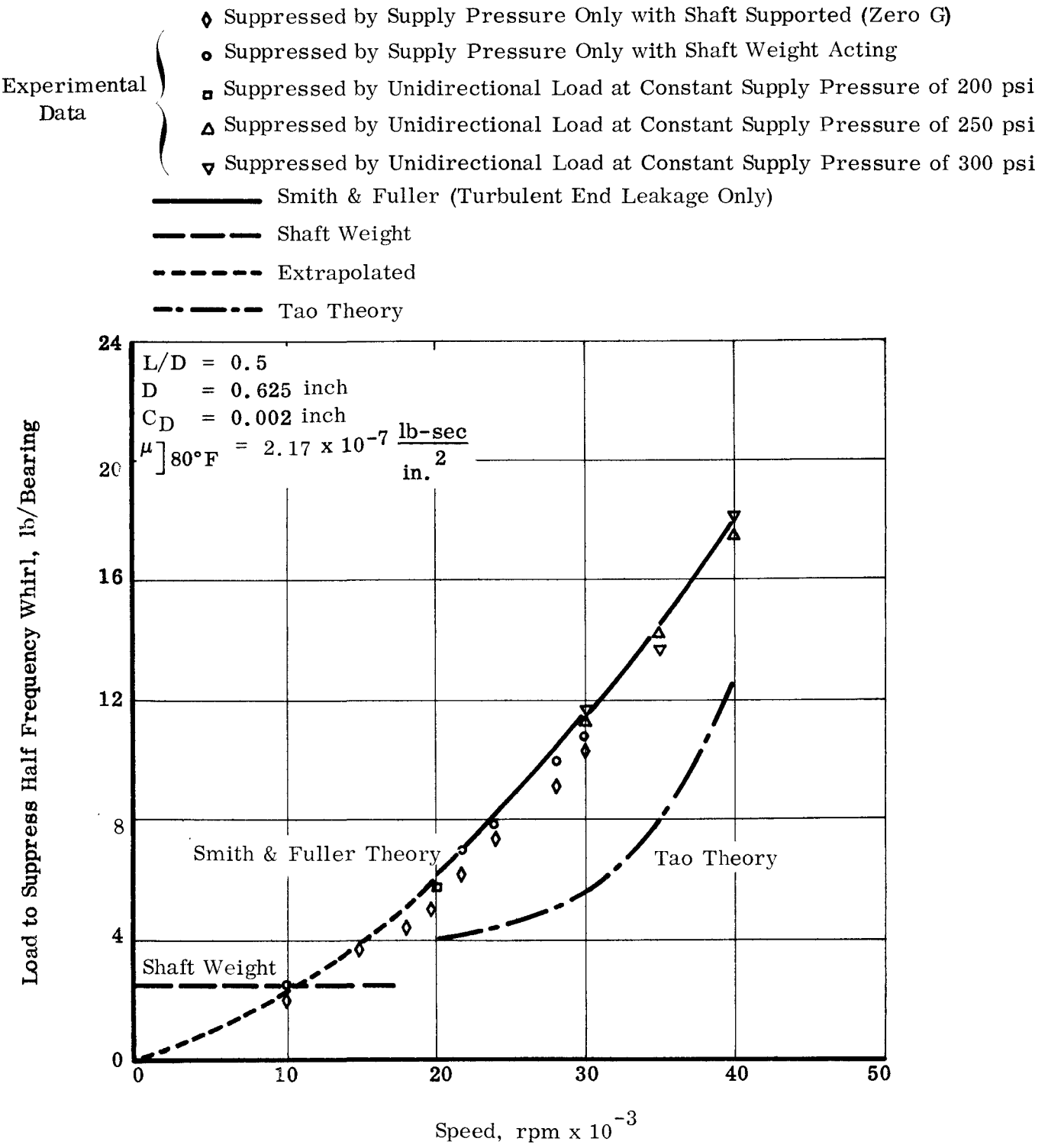

Figure 14. Experimental and Theoretical Whirl Characteristics Showing Load to Suppress Half-Frequency Whirl for Turbulent Flow Plain Journal Bearing

Since for speeds up to 40,000 rpm the radial stiffness for eccentricity ratios of $\epsilon < 0.5$ was very much lower (by a factor of 10 or more) than the shaft stiffness, the stability characteristics were established neglecting shaft stiffness.

$$\omega_{cr} \leq 2 \sqrt{\frac{K_r}{M}} \text{ rad/sec in the limit (see Volume I, Paragraph III-C-5) . . . 2}$$

The good agreement obtained between actual threshold data and that predicted by analysis using the technique developed in Volume I, Paragraph III-C-5 provides confidence in the approach and in the measurements made during actual tests.

As stated above, operation of mercury lubricated bearings with turbulence is possible without destructive results. Speed can be increased even though the threshold of instability has been passed and the shaft is whirling at half-frequency. This procedure is not without considerable risk. This is indicated in Figure 15, which presents the whirl amplitude (both synchronous and half-frequency) as a function of speed for various supply pressures, i.e., internal loads. The fundamental component is very small in comparison to the rapidly increasing half-frequency components, indicating excellent balancing. The rate of growth of the half-frequency component shows that even though speed can be increased once the threshold is reached, the whirl amplitude soon approaches the total bearing clearance, and it is only the squeeze film action and the damping of the film which prevents bearing failure.

The influence of a rotating load, equivalent to an unbalance of 30 lb/bearing at 40,000 rpm established during BETR 4A, is shown in Figure 16. This figure shows the lower whirl threshold of the unbalanced rotor and the rapidly rising whirl amplitude with small increases in speed. The synchronous component is also greater than the balanced case, as expected. Each supply pressure does, however, have a distinguishable characteristic. With unidirectional load (due to supply pressure) superimposed on the rotating load vector (due to unbalance), the shaft orbit is distorted into an elliptical locus. Consequently, it becomes difficult to establish actual whirl amplitude. This may explain the slight variation in peak amplitude recorded for different supply pressures.

E. POWER LOSS

The turbulent power loss predicted by Wilcock and Booser and that based on the experimental work of Smith and Fuller agree fairly closely over the range of Reynolds numbers encountered in the SNAP 2 applications. Figures 17 and 18 show the turbulent correction factors to be applied to the laminar Petroff power loss by these two separate investigations.

Figure 17 shows the turbulent power loss predicted by the use of the turbulent "j" factor derived by Wilcock and Booser. Experimentally determined power loss values are also shown for a series of plain bearings having a diameter of 0.625 inch and a length of 0.312 inch with diametral clearances varying from 0.0014 inch to 0.002 inch. The measured power loss follows the predicted trend, but is slightly greater. As anticipated

(Amplitudes Obtained From Bruel & Kjoer Wave Analyzer.
Input is Obtained From Alternator Vertical Capacitance Probe.)

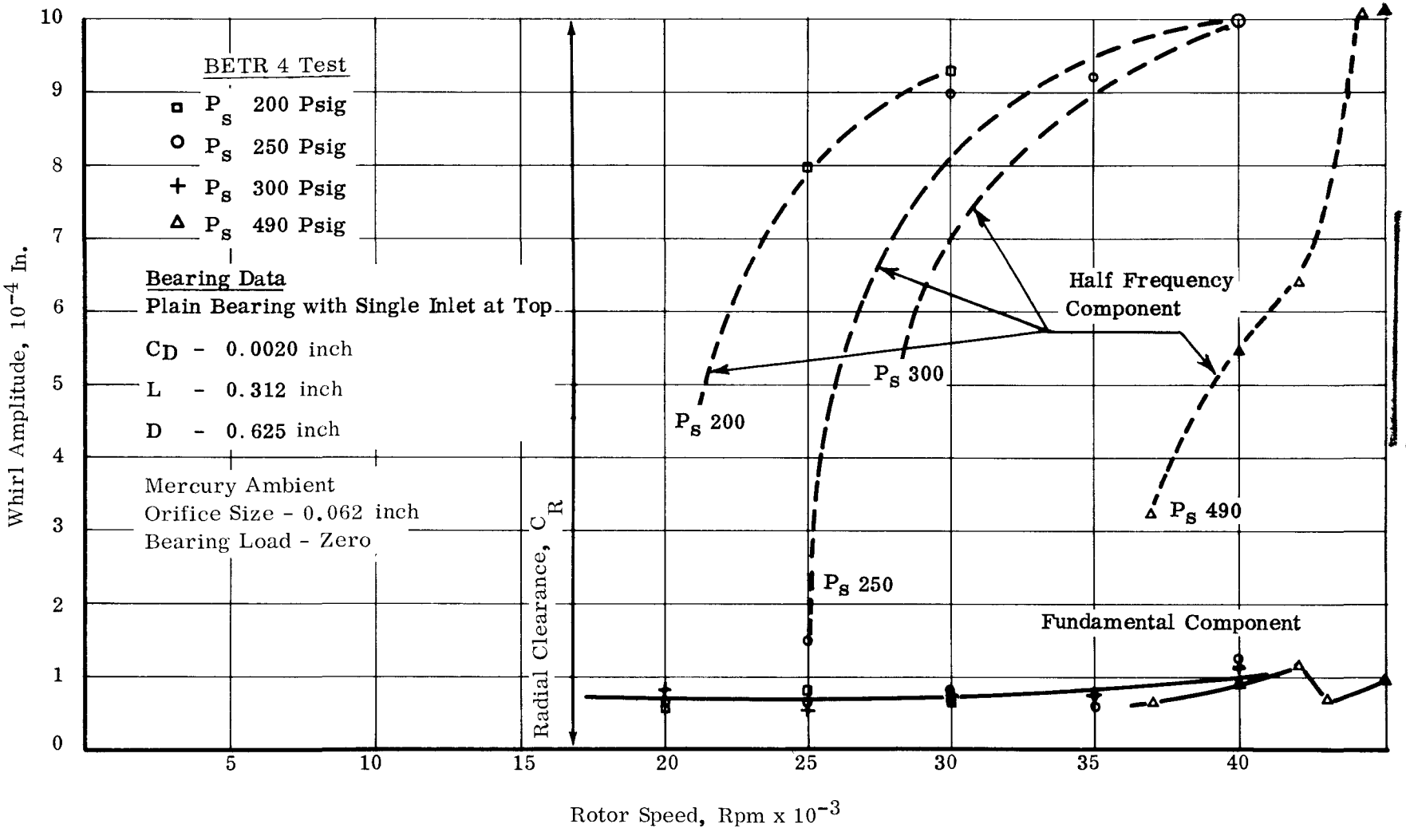

Figure 15. Whirl Amplitude vs Rotor Speed for Plain Bearing

(Amplitudes Obtained From Bruel & Kjoer Wave Analyzer.
Input is Obtained From an Alternator Vertical Capacitance Probe.)

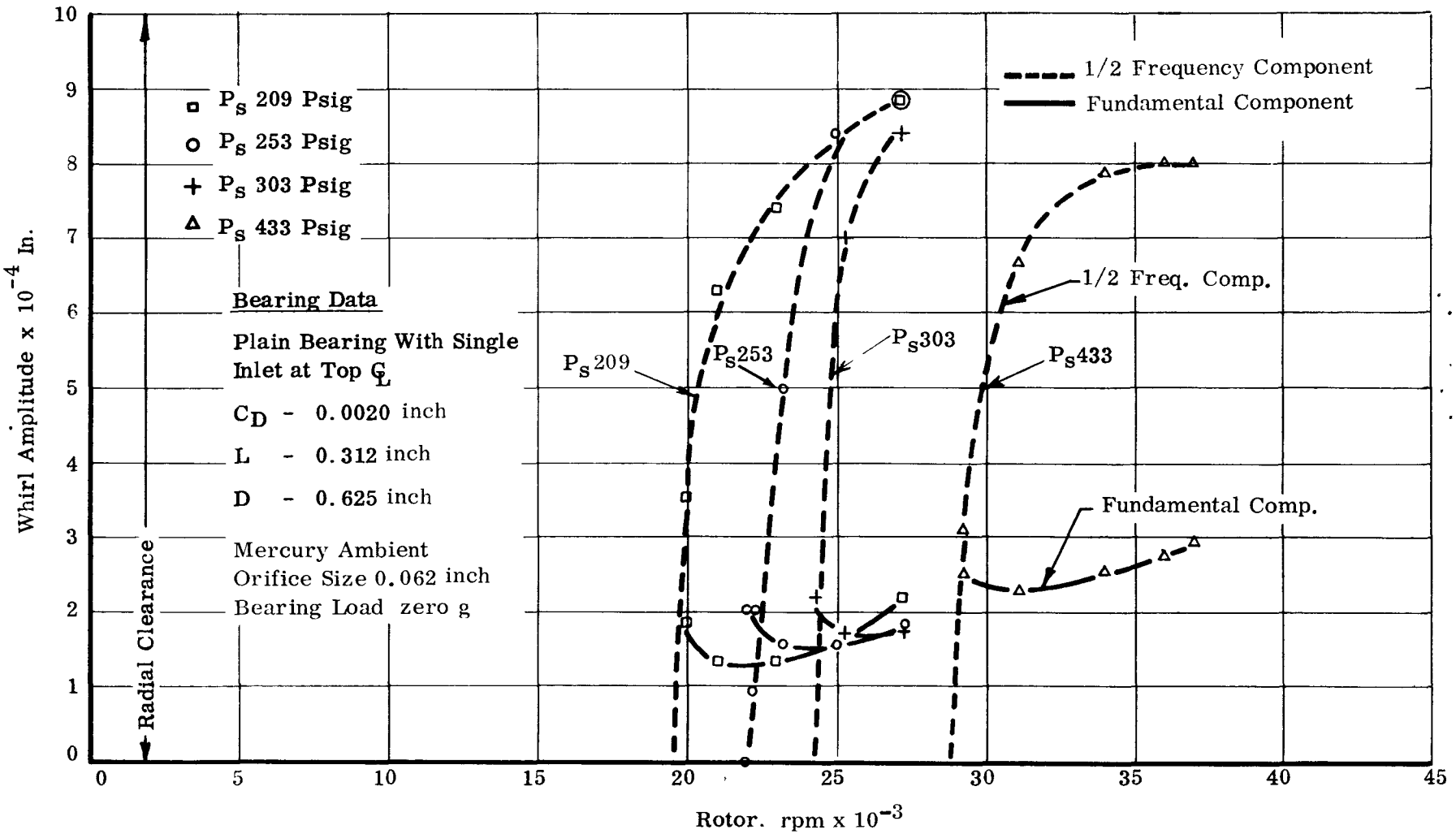

Figure 16. Whirl Amplitude vs Rotor Speed for a Plain Bearing
With 30 lb/bearing Unbalance at 40,000 rpm

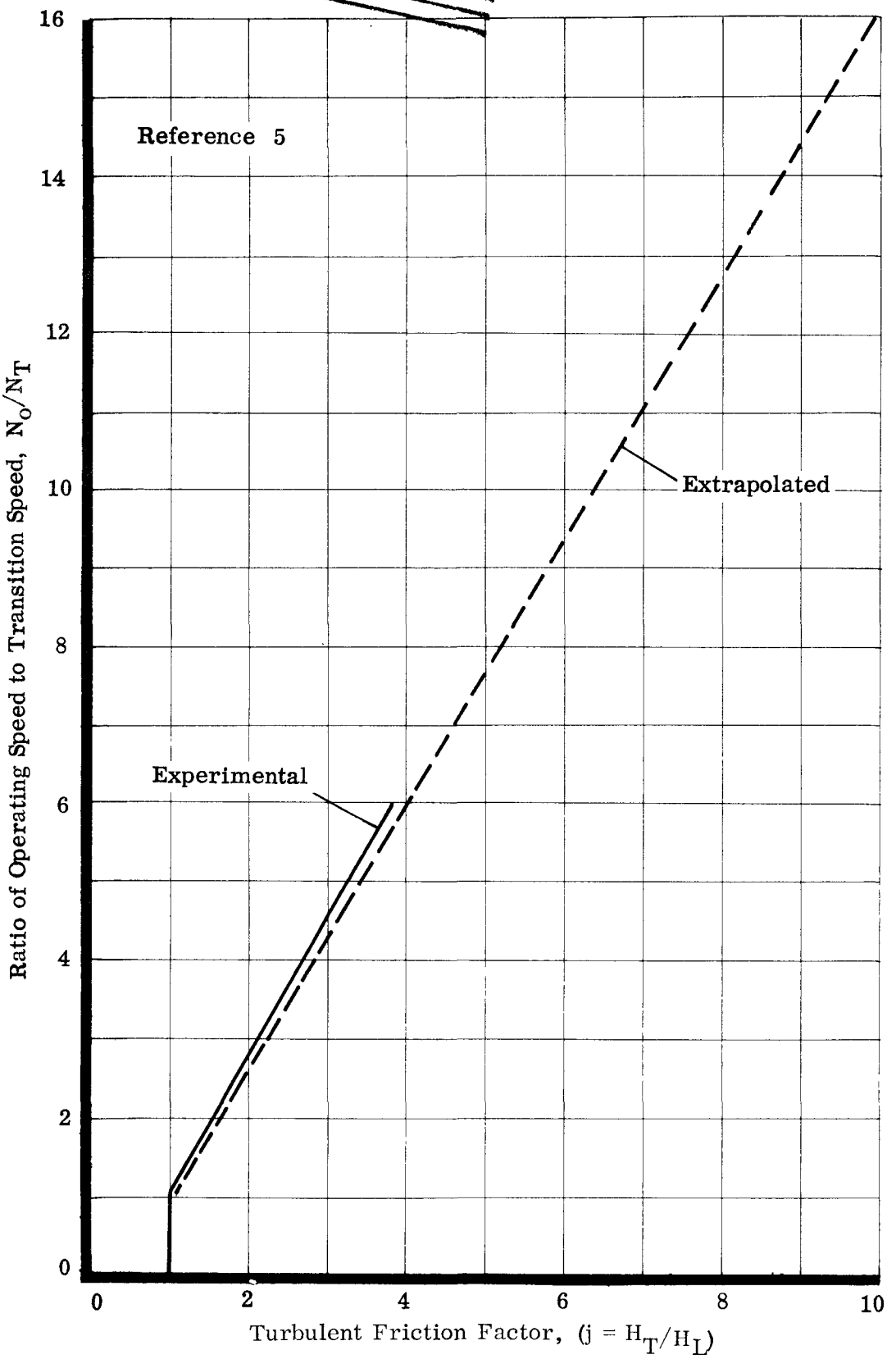

Figure 17. Power Loss Factor for Journal Bearings Operating in the Turbulent Regime

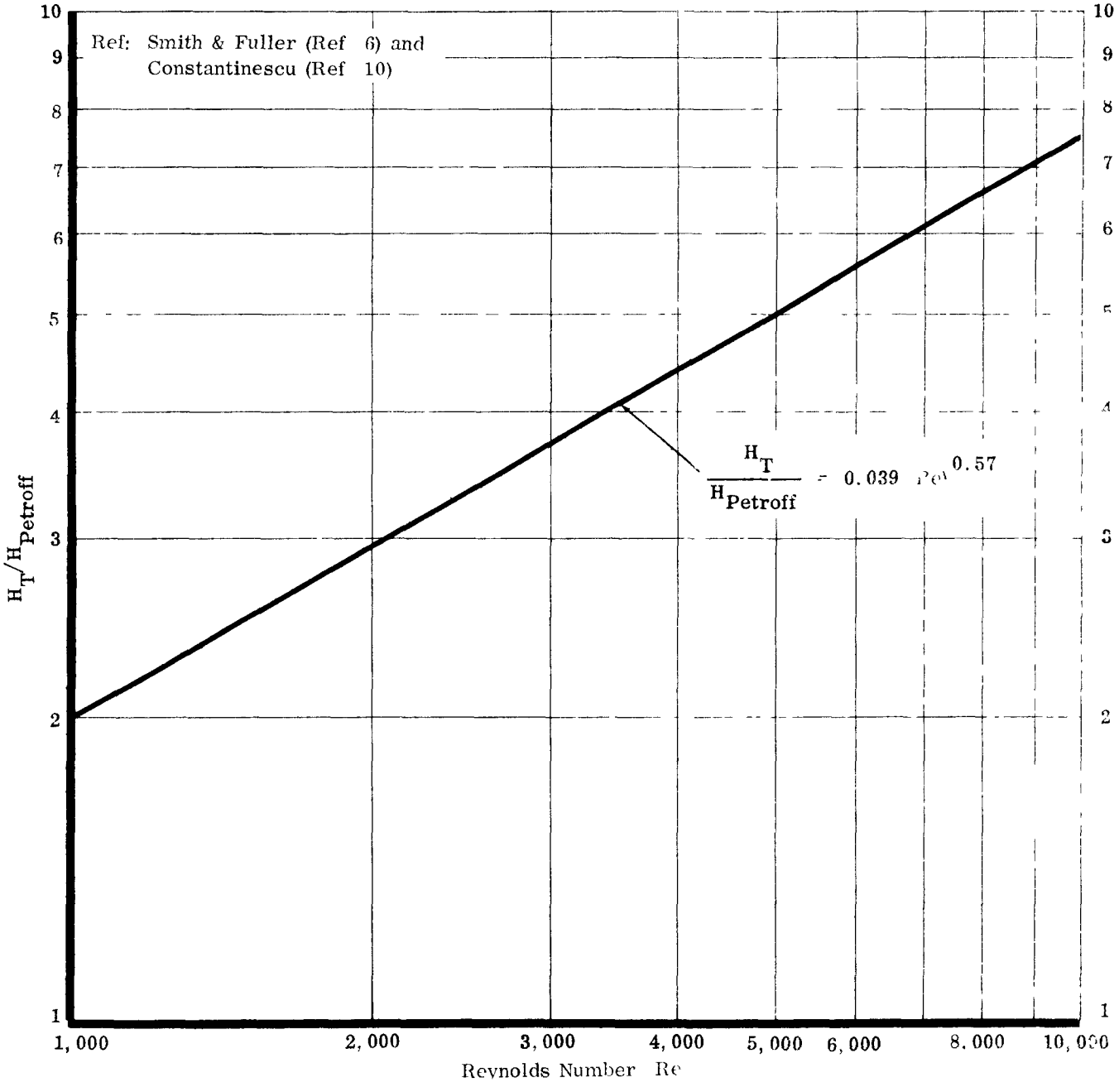

Figure 18. Power Loss Factor vs Reynolds Number for Journal Bearings Operating in the Turbulent Regime

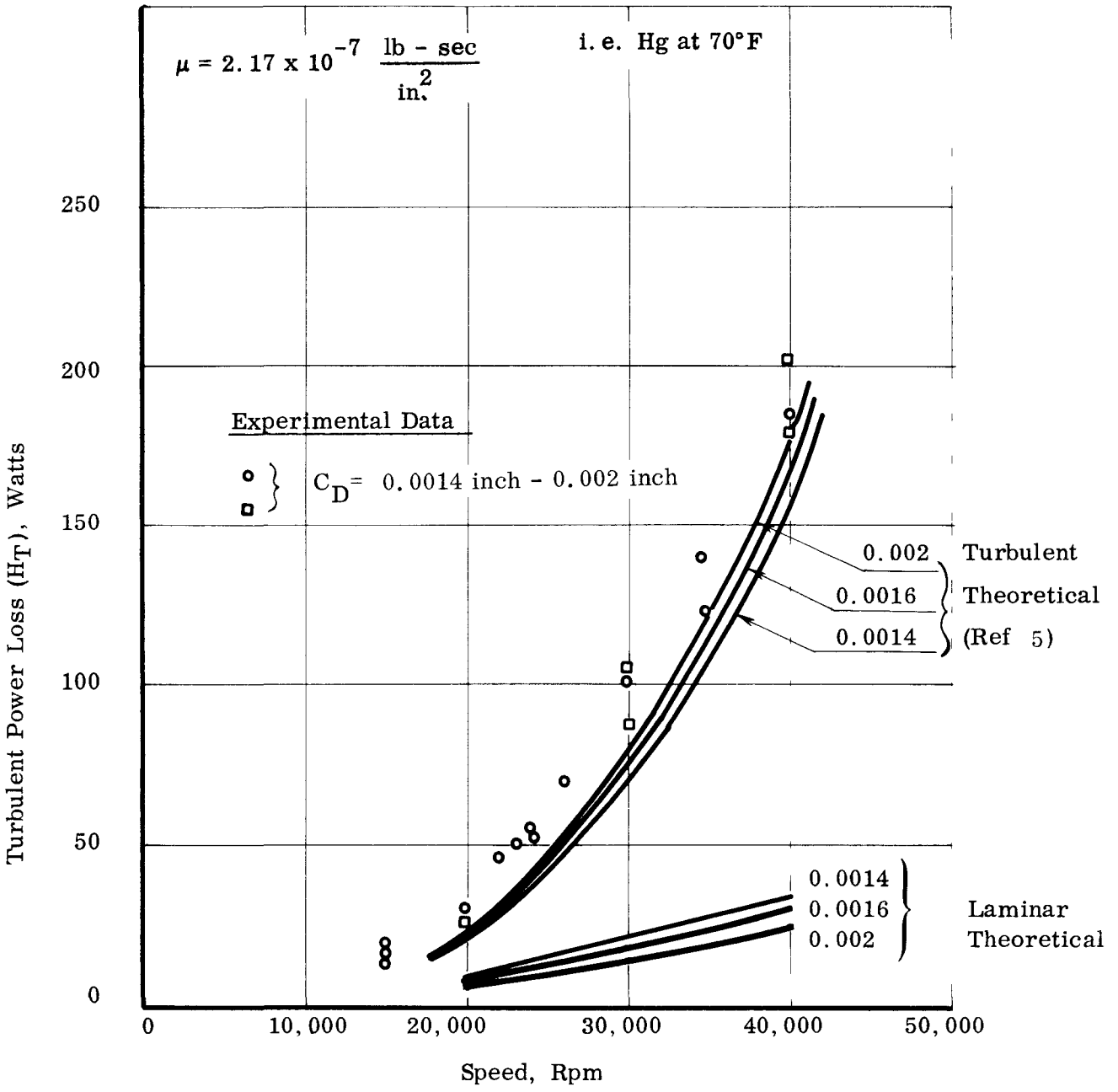

Figure 19. Experimental and Theoretical Turbulent Power Loss for 0.625-Inch Diameter, 0.312-Inch Length Plain Bearing

it is almost an order of magnitude greater than power loss based on laminar flow predictions. The determination of power loss is important in establishing the overall efficiency of the package, and, consequently, measurements by dynamometer and speed-decay methods are geared to the desired accuracy. This is predicted to be ± 20 watts at 40, 000 rpm.

Figure 19 points out the minor effects that diametral clearance has on power loss for the turbulent flow bearing. Laminar theory predicts that power loss increases directly with decreasing clearance. That this is not the case for turbulent flow is demonstrated analytically using the Wilcock and Booser approach. The turbulent power loss predicted in this manner shows that over the range of clearances evaluated in this application the power loss actually decreases with decreasing clearance, although the reduction is not great. The reason for this result is again due to the Reynolds number effect on the degree of turbulence in the bearing. Since Reynolds number decreases with bearing clearance, the transition speed for onset of turbulence increases. Consequently the ratio of operating speed to transition speed decreases and a lower "j" factor results.

The result is that the correction for turbulent flow drops more rapidly than the increase in laminar power loss, with the net effect of lower power loss for smaller clearance bearings. Experimentally, the measurement of power loss did not indicate a significant difference with changing clearance from 0.0014 to 0.002 inch for the plain bearing. For the 0.002-inch plain bearing at 40, 000 rpm, the laminar prediction was 25 watts, the turbulent prediction was 180 watts, and the measured value varied between 175 and 200 watts.

Calculating predicted turbulent power loss utilizing Smith and Fuller's experimentally determined relationship results in a reverse trend with clearance, as shown in Figure 20. Consequently the trend is in the same direction as that predicted by laminar theory; i.e., power loss decreases with increase in clearance. This is to be expected since the turbulent power loss is a weaker function of Reynolds number than the laminar power loss, as predicted by the equation

$$H_T = H_L \times 0.039 \times (Re)^{0.57}.$$

At $C_D = 0.002$ the predicted value based on both Wilcock and Booser and Smith and Fuller agrees within a few watts.

The experimental data from Figure 19 are repeated in Figure 20 and show satisfactory correlation with the Smith and Fuller predicted values. For the 0.002-inch clearance plain bearing evaluated, the turbulent prediction at 40, 000 rpm was 168 watts, while the measured value varied between 175 and 200 watts.

Figure 21 shows the total power loss measured for two plain bearings and one double acting thrust bearing. The predicted laminar power loss for the spiral groove thrust bearing was 20 watts at 40, 000 rpm. The measured value was approximately 100 watts per side. These high power losses play major roles in establishing the final size of the bearings.

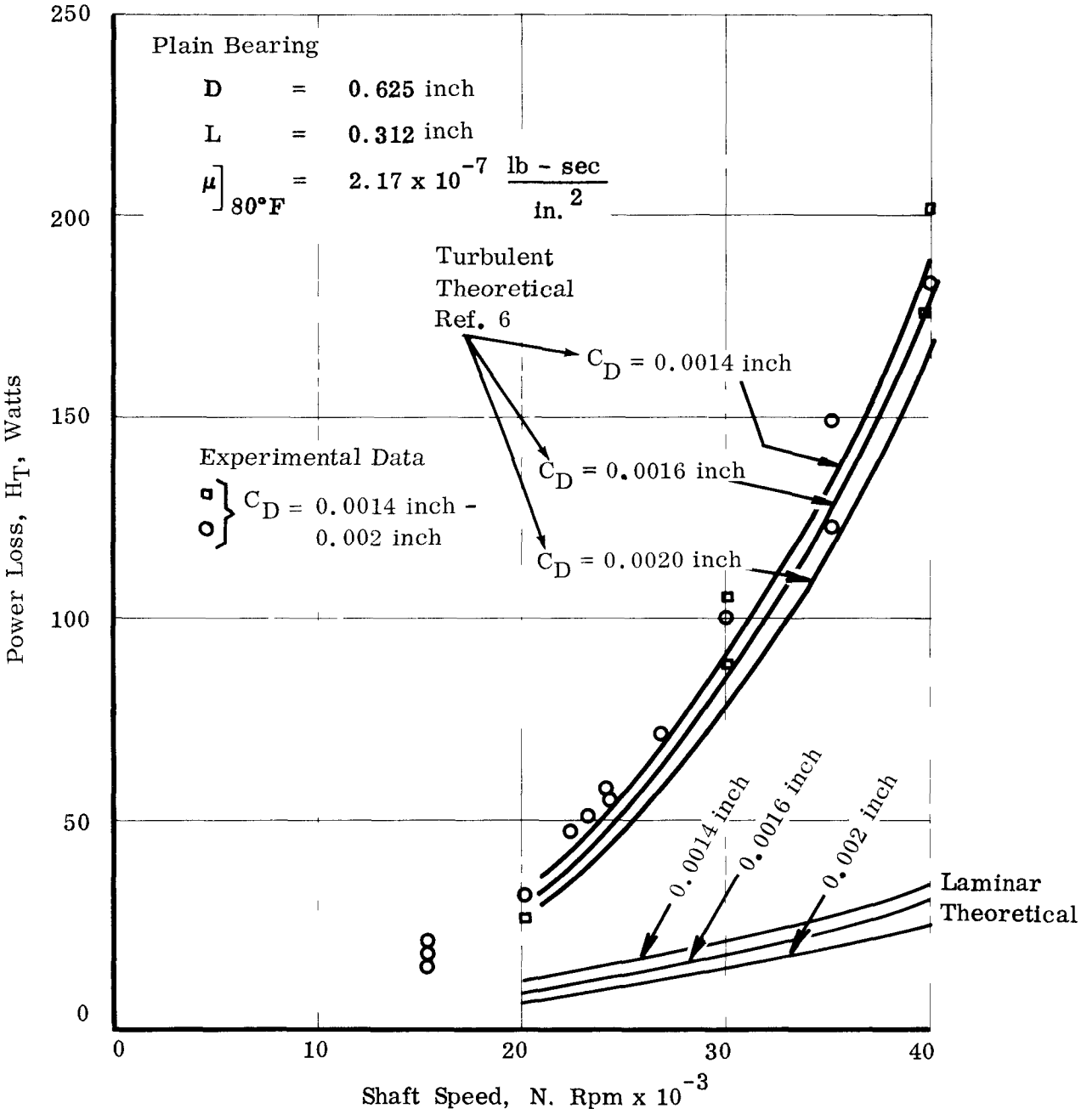

Figure 20. Experimental and Theoretical Power Loss for a Plain Journal Bearing Based on Smith and Fuller Data

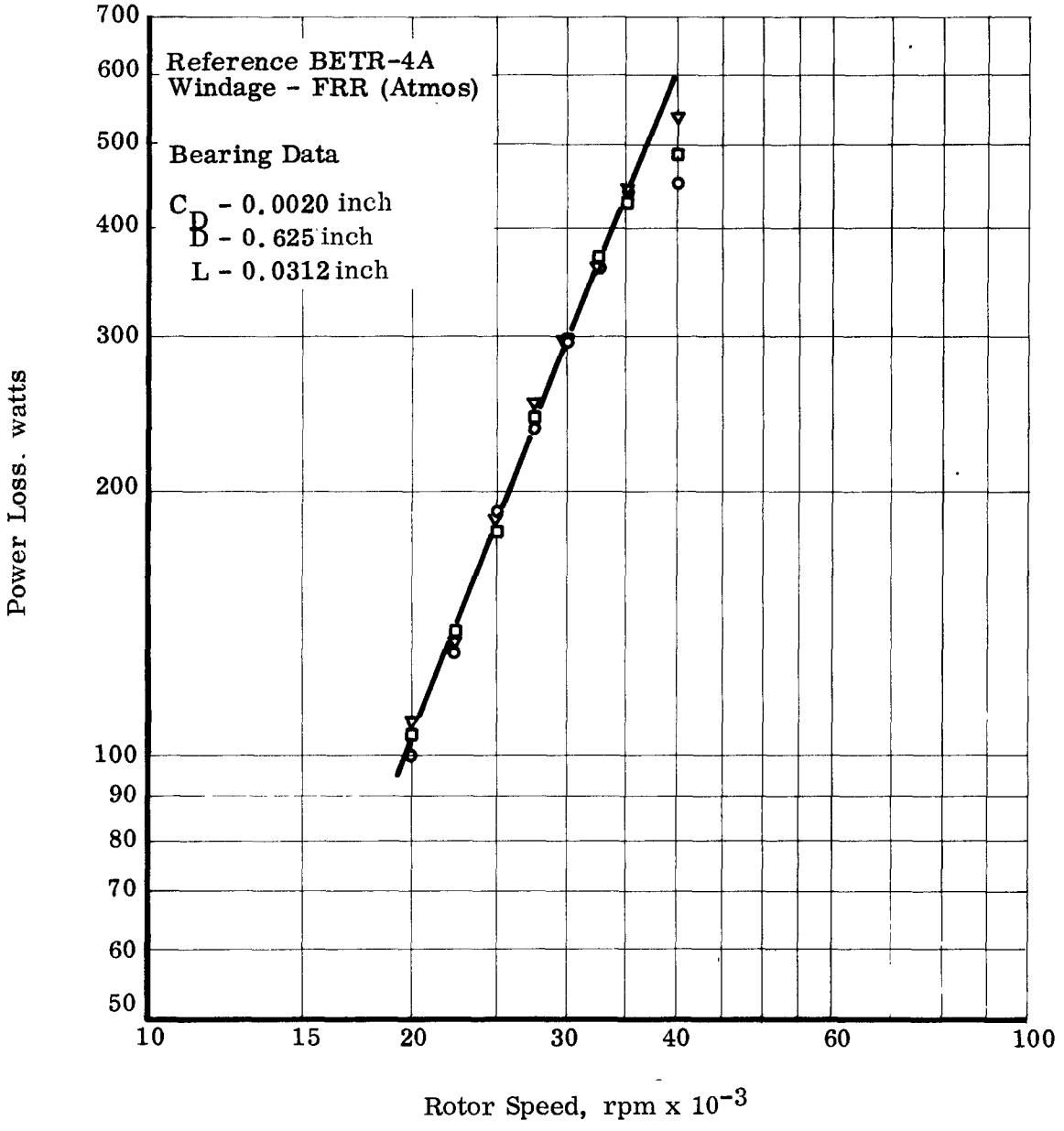

Figure 21. Bearing Power Loss vs Rotor Speed for Two Plain Bearings and One Spiral Groove Thrust Bearing

F. FLOW

Since the initial effort for predicting bearing performance was based on the "short bearing approximation" the work of DuBois and Ocvirk was used to define the flow factor, q. Figure 22 shows q as a function of a modified Sommerfeld number which includes supply pressure where q is a function of $1/C_R \times W/LD \times 1/P_s$. The eccentricity ratio is determined from the DuBois and Ocvirk $1/C_n$ vs ϵ curve.

Utilizing the technique devised by Wilcock and Booser yielded predictions at complete variance with observed results. Figure 23 shows the difference both in magnitude of flow rates and trend effects of supply pressure and speed. Initially, a major problem proved to be the predictability of this operating clearance of the bearing. Both contaminants (rust or mercury oxide) and consistent differential thermal expansion caused difficulties. Analytical prediction of flow rate consequently assumed secondary importance, and attempts were made to improve the reproducibility of experimental results.

Figure 24 shows a typical plot of the flow-pressure relationship as a function of speed for the plain bearing type. Because of the many factors involved, correlation of the experimental results with analytical predictions is virtually impossible on a generalized basis. It is reasonable to expect that flow rate will be at least a function of clearance, speed, supply pressure, eccentricity ratio, feed groove configuration, and viscosity. However, clearance and viscosity will be affected by temperature which, in turn, is a function of power loss. The eccentricity ratio is a function of load, which is affected by the supply pressure in this particular bearing configuration. Moreover, flow will be affected by an orbital motion of the shaft as in half-frequency whirl. Consequently, prediction of flow has to be based on tests of specific bearings.

For the particular bearing data shown in Figure 24, the flow rates for the non-rotating and rotating cases appear to be represented by the following relationships:

$$Q_o = 0.475 P_s^{0.65} \text{ lb/min} \quad \ldots 4$$

and

$$Q_N = 357 N^{-1.24} P_s^{1.5} \text{ lb/min} \quad \ldots 5$$

Where Q_o = flow at zero speed

and Q_N = flow at speed N rpm

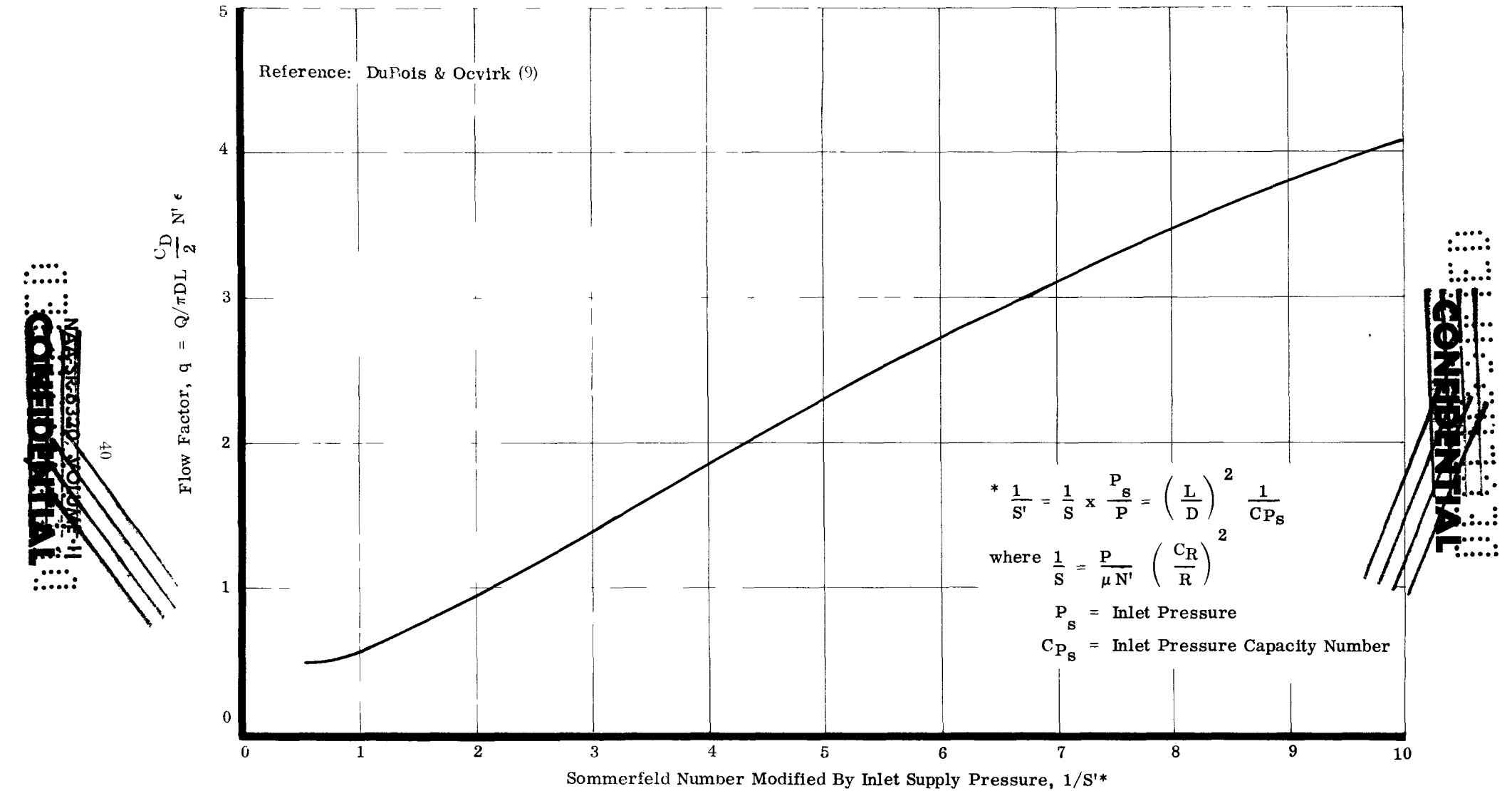

Figure 22. Flow Factor for a Short Journal Bearing

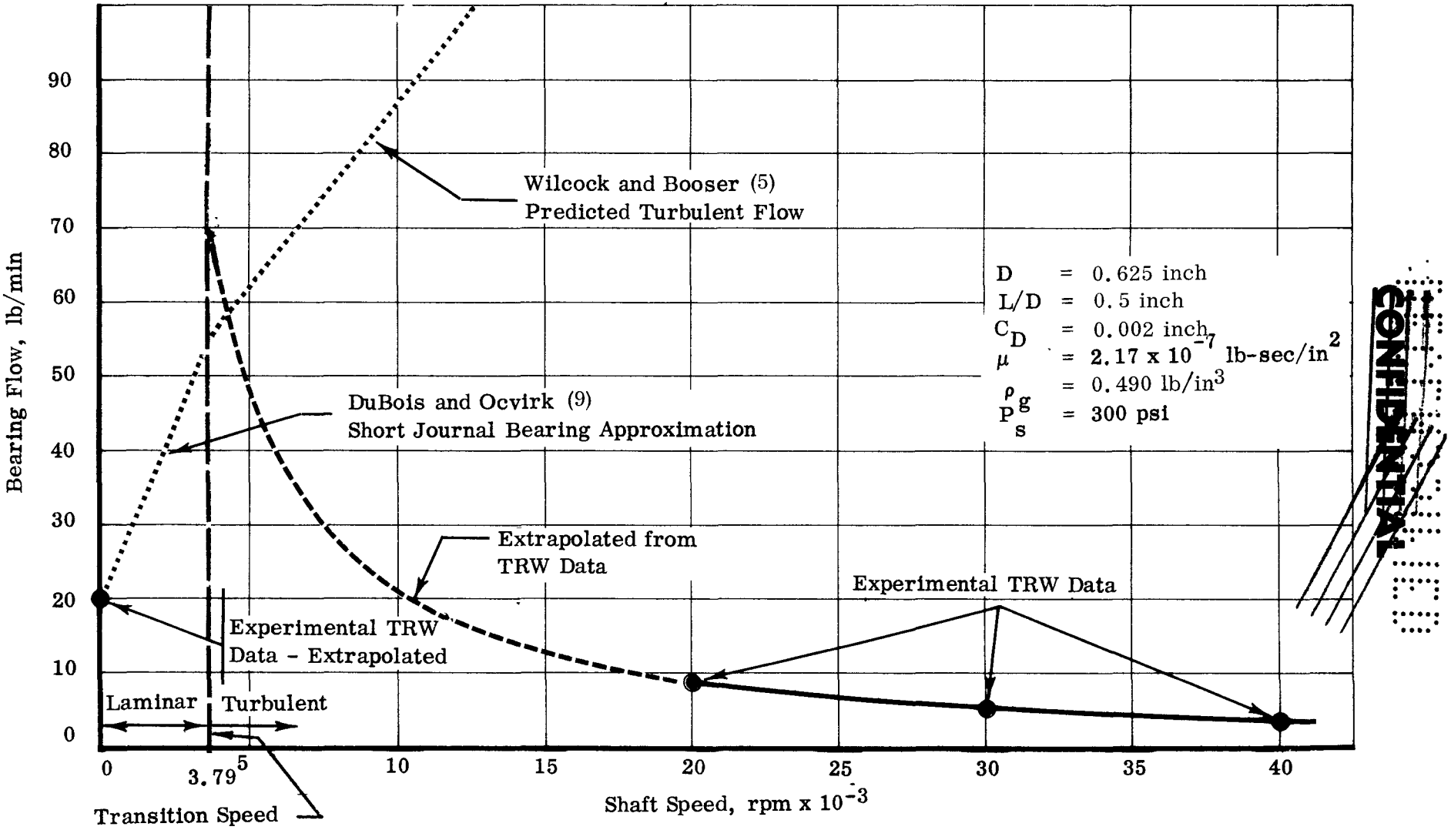

Figure 23. Bearing Flow vs Shaft Speed for a Plain Journal Bearing

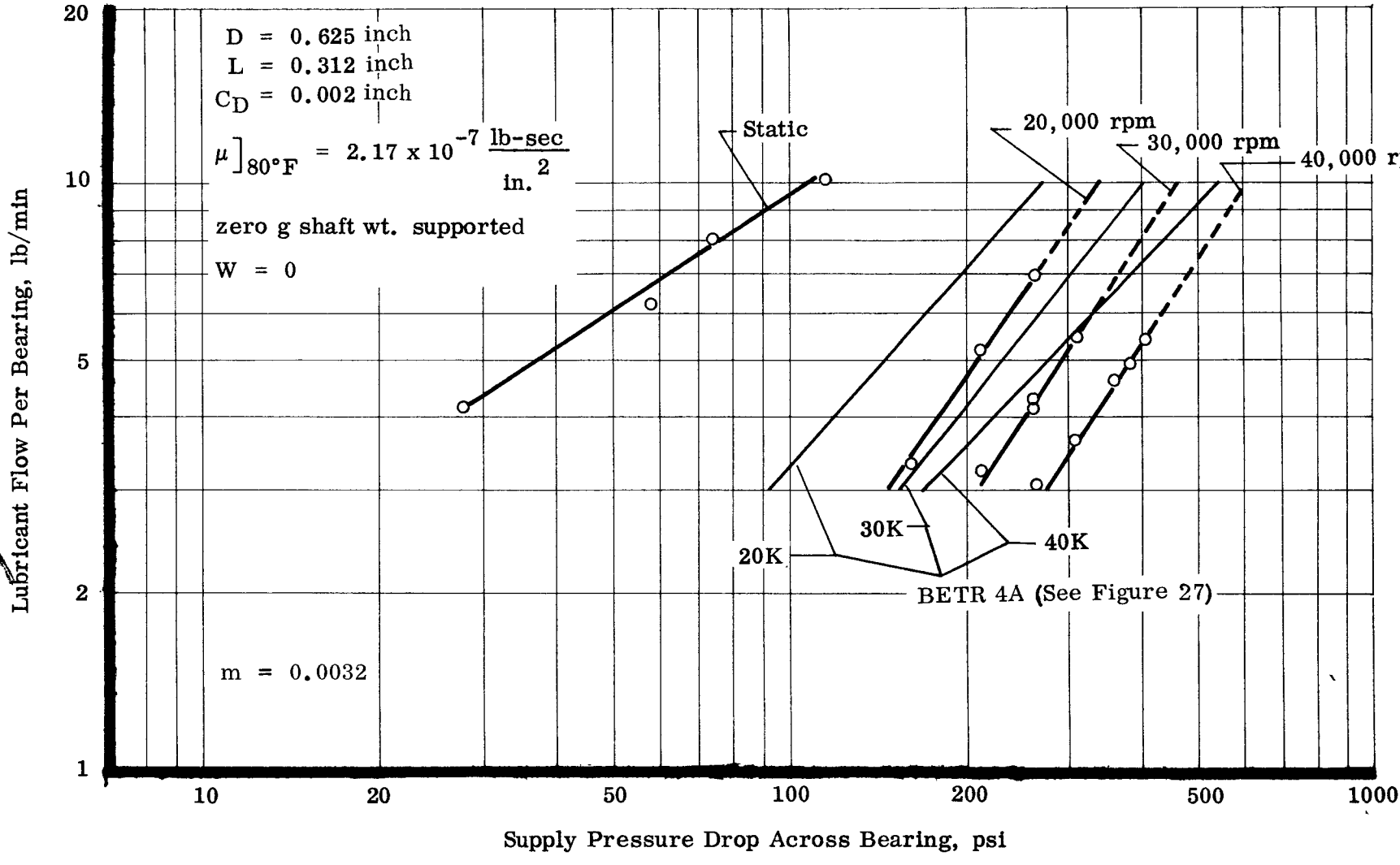

Figure 24. Experimental Flow Characteristics for a Plain Journal Bearing (Turbine End)
(L/D = 0.5)

If the flow rate is computed for the laminar short journal bearing (Reference 9), taking into account the loading due to the supply pressure, several observations may be noted:

1) That flow rate in the non-rotating case does not follow the Hagen-Poiseuille law of equation (6) is to be expected, because the assumed mid-plane circumferential feed groove has been replaced by an axial groove. However, the flow rate does not vary linearly with supply pressure and is less, rather than greater, for a given pressure.

2) At high supply pressures, over 200 psi, speed has little effect on the predicted flow for the laminar case (equation (5) with N substituted for N_{tr}) since the product of the flow factor, q, and the eccentricity ratio are nearly constant. Eccentricity ratio is determined for the corresponding reciprocal Sommerfeld number from Figure 6. A flow reduction in the turbulent case is expected with an increase in speed, since the degree of turbulence is increased.

Theory predicts that for turbulence the total flow for a given supply pressure and speed is less than when flow remains laminar. This has been verified experimentally by the extremely high pressure required to pass flow through the bearing. Theoretical prediction of flow for this type of bearing size, assuming laminar conditions (which naturally do not exist) called for a supply pressure of 150 psi in the concentric case, with a flow of 6.0 lb/min at 40,000 rpm. Actual pressure to pass 6.0 lb/min through the bearing was measured at 440 psi.

For the plain journal bearing with the supply pad on top, flow characteristics behave as anticipated. As downward load is increased, flow increases rapidly for a constant pressure since the restriction is not in the orifice but in the annulus created by the bearing clearance space and the supply pad. Consequently, it reaches a maximum with the shaft displaced the maximum amount in the bearing. Figure 25 shows this influence and the region of stable and unstable operation. However, loading the shaft into the supply pad quickly throttles the flow as eccentricity ratios become negative, i.e., loading upward. The pressure in the supply recess does not increase since it is not orifice-compensated or constant flow-controlled. This can be a serious problem should the upward load exceed the ability of the hydrostatic pressure forces to keep the journal below the center. Such loads can be obtained in this application as a result of large dynamic rotating loads. Under those circumstances the flow would tend to be pulsating.

Figure 26 shows the influence of the magnitude and direction of the applied unidirectional load on the flow characteristics of the plain bearing at 30,000 rpm. The total load would be the sum of the unidirectional (externally applied) load and the internal load due to the high pressure source at the top of the bearing.

(Does Not Include Loads Applied by Lube Supply Pressure.
Direction is In-Line with Lube Supply Pad)

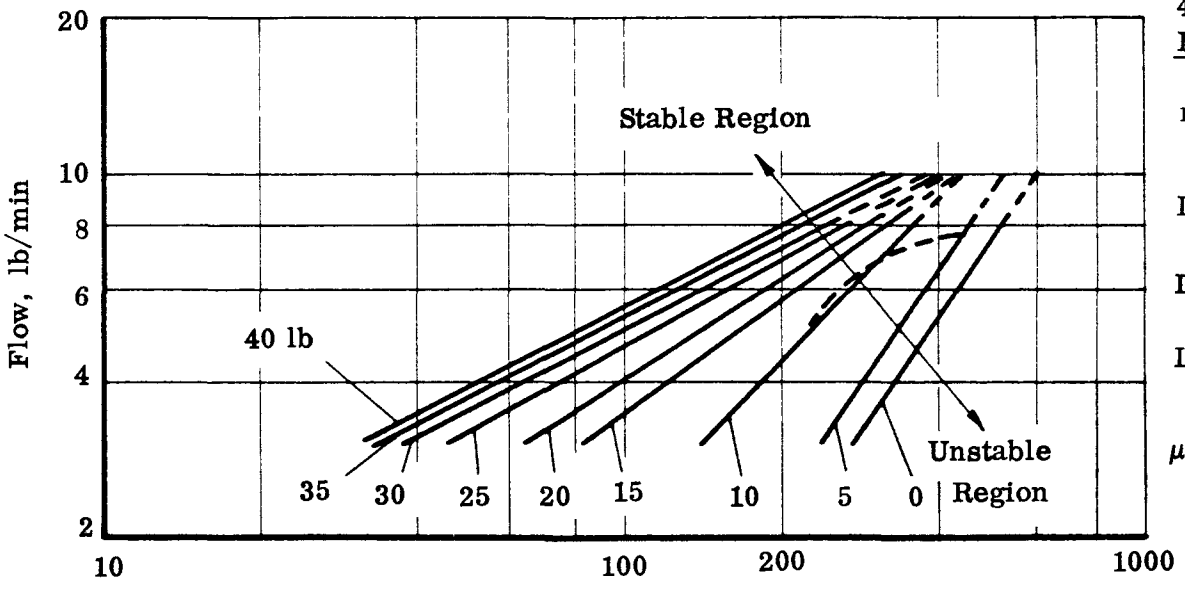

40,000 rpm
Bearing Data:

$m = 0.0032 = \frac{C_D}{D}$

$L/D = 0.5$

$D = 0.625$ inch

$L = 0.312$ inch

$\mu]_{80°F} = 2.17 \times 10^{-7} \frac{\text{lb-sec}}{\text{in.}^2}$

Figure 25. Flow Pressure Relationship for Plain Bearing with Downward Unidirectional Loads at 40,000 rpm

Bearing Data

Plain with One Inlet at Top (Turbine Bearing)

C_D = 0.0020 inch

D = 0.625 inch

L = 0.312 inch

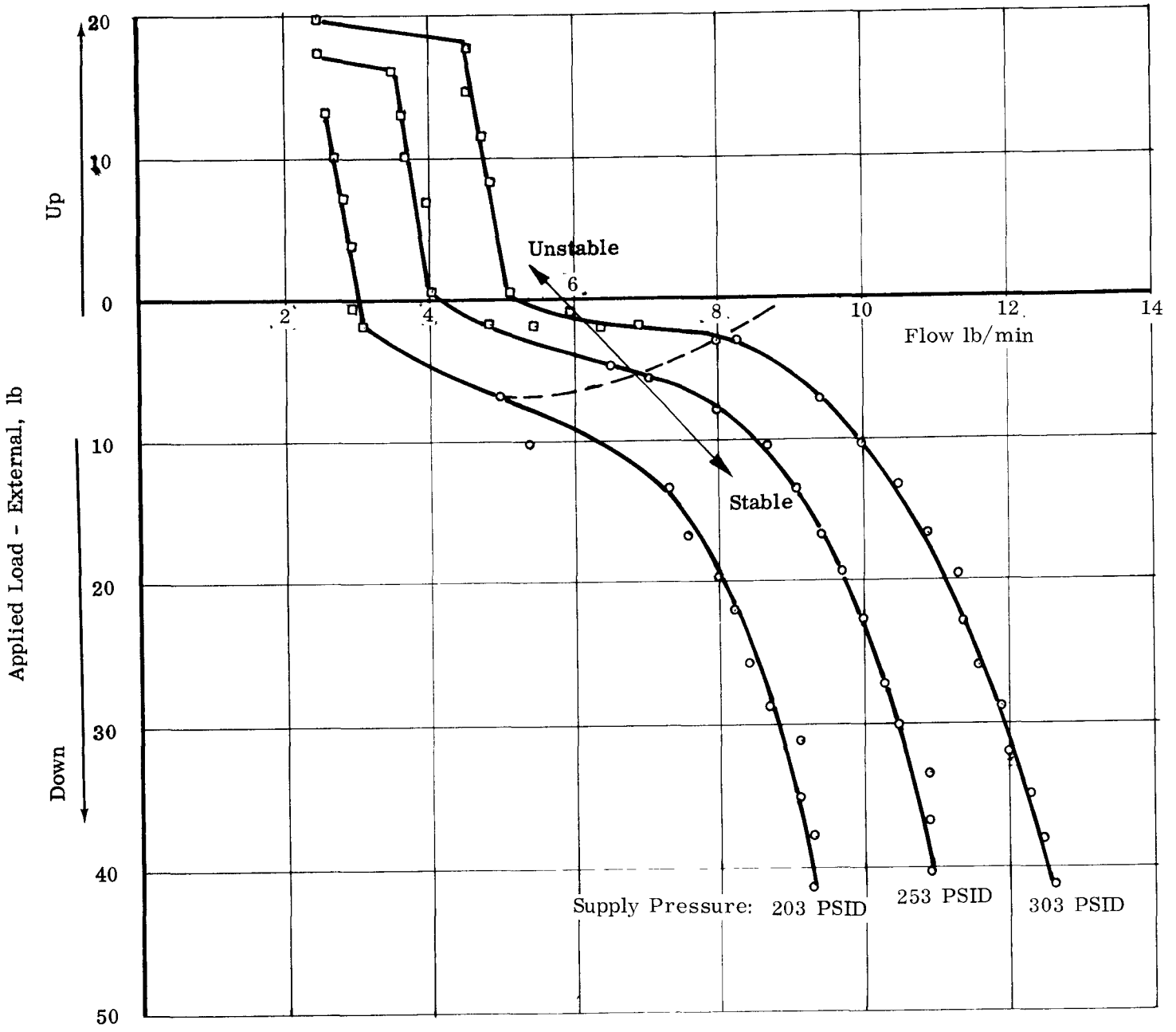

Figure 26. Load vs Flow at 30,000 rpm

Limits of stability at 30,000 rpm are also shown in Figure 26. As half-frequency whirl is encountered the flow drops rapidly for constant supply pressures. Loading upward, to "negative" eccentricity ratios, does not improve stability, but the rate of flow falloff is less. The limiting load applied upward into the single supply pad is shown as the final rapid falloff in flow. For the supply pressures of 203, 253, and 303 psid, the limiting upward load before flow is choked off is 13, 16, and 18 lb, respectively. This limitation clearly illustrates the preferential load orientation of this type of bearing and its sensitivity to rotating loads.

The need for self-compensation by means of orifice restriction will be discussed later, but it can be seen that such provisions would reduce the seriousness of this problem.

G. INFLUENCE OF ROTATING LOADS

The addition of a rotating load equivalent to 30 lb/bearing at 40,000 rpm was evaluated in BETR 4A. The bearings remained unchanged. The influence on flow-pressure-speed performance is shown in Figure 27. For a given flow, the required pressure is considerably less than in the balanced case, and the slope of the curve has changed. The addition of rotating loads and the subsequent greater synchronous whirl orbit therefore influences the flow characteristics in the same way that an applied unidirectional load away from the supply pad does. These data are superimposed on Figure 24.

The influence of unidirectional load, superimposed on the rotating load at 30,000 rpm, is shown in Figure 28. This is similar to the balanced rotor except that the onset of instability is not indicated by a marked change in flow-pressure. Since there is a large synchronous component present even during stable operation, this variance with the balanced case when encountering whirl is to be expected.

The influence of a 60 lb/bearing rotating load at 40,000 rpm was evaluated in BETR 4B. The maximum speed attained was 30,000 rpm, then the bearing failed due to excessive loads. The combined load at the instant of failure was 31 lb/bearing unidirectional plus some 35 lb/bearing rotating. Prior to the failure several significant performance parameters were established.

Figure 29 show the static and dynamic (20,000 and 30,000 rpm) flow characteristics. Slopes are again different, but the reversed trend from balanced to 30 lb/bearing unbalance is more significant. Lower pressures were required for the 30 lb/bearing unbalance than for the balanced rotor. At 60 lb/bearing unbalance, much higher pressures are required for high flows than for the balanced rotor. At low flows, however, a lower pressure is required at 30,000 rpm.

The influence of load on flow at constant pressure at 20,000 rpm is shown in Figure 30. The characteristic is identical to the balanced rotor except that flow is considerably less for a given load and pressure. The larger synchronous component is responsible for this.

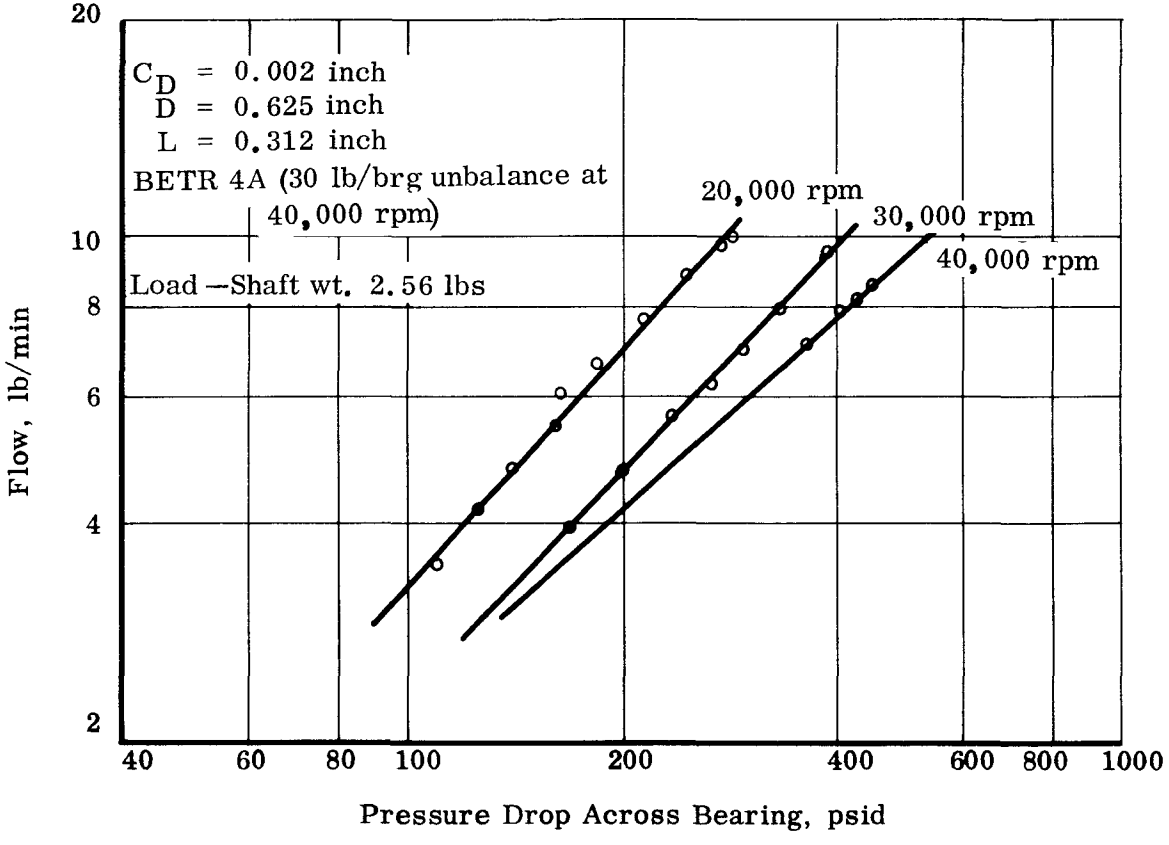

Figure 27. Flow Calibration for a Plain Bearing with a Single Inlet at the Top Bearing - Turbine

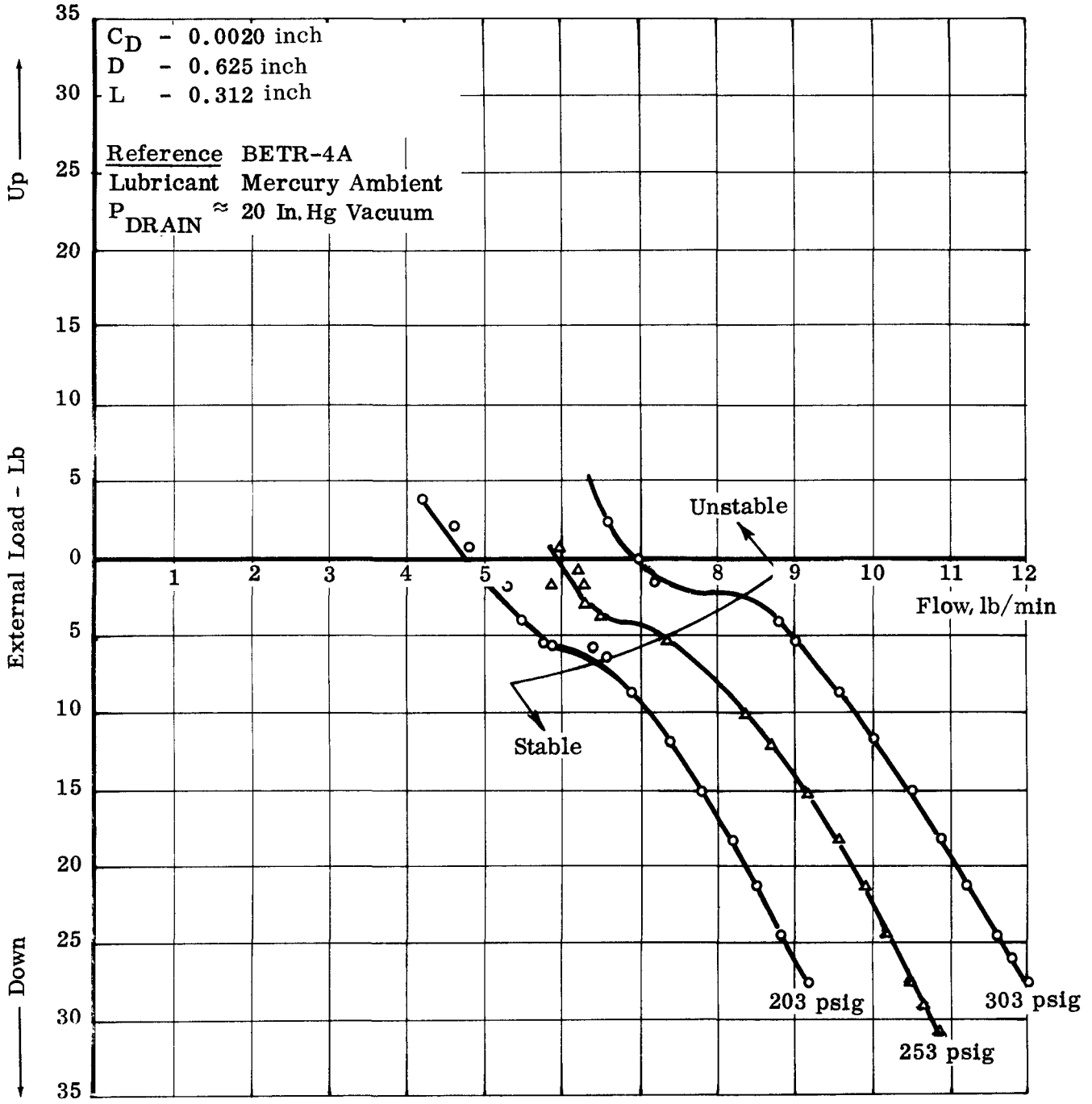

Figure 28. Load vs Flow at 30,000 rpm Plain Bearing with Single Inlet at Top ℄ (30 lb/Bearing Rotating Load at 40,000 rpm) (Turbine Bearing)

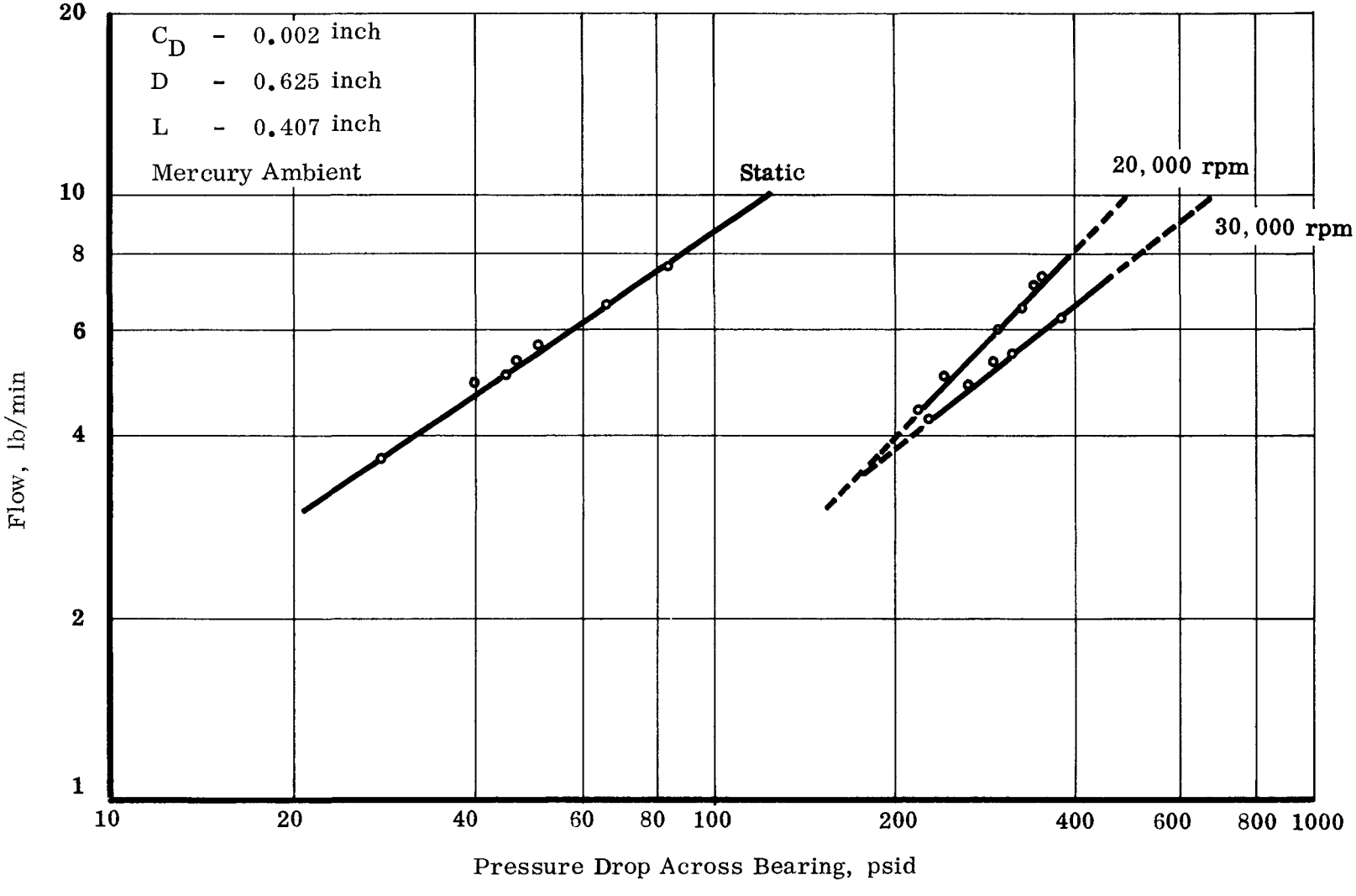

Figure 29. Load vs Flow for a Plain Bearing With a Single Inlet at the Top Test BETR 4B (Turbine Bearing)

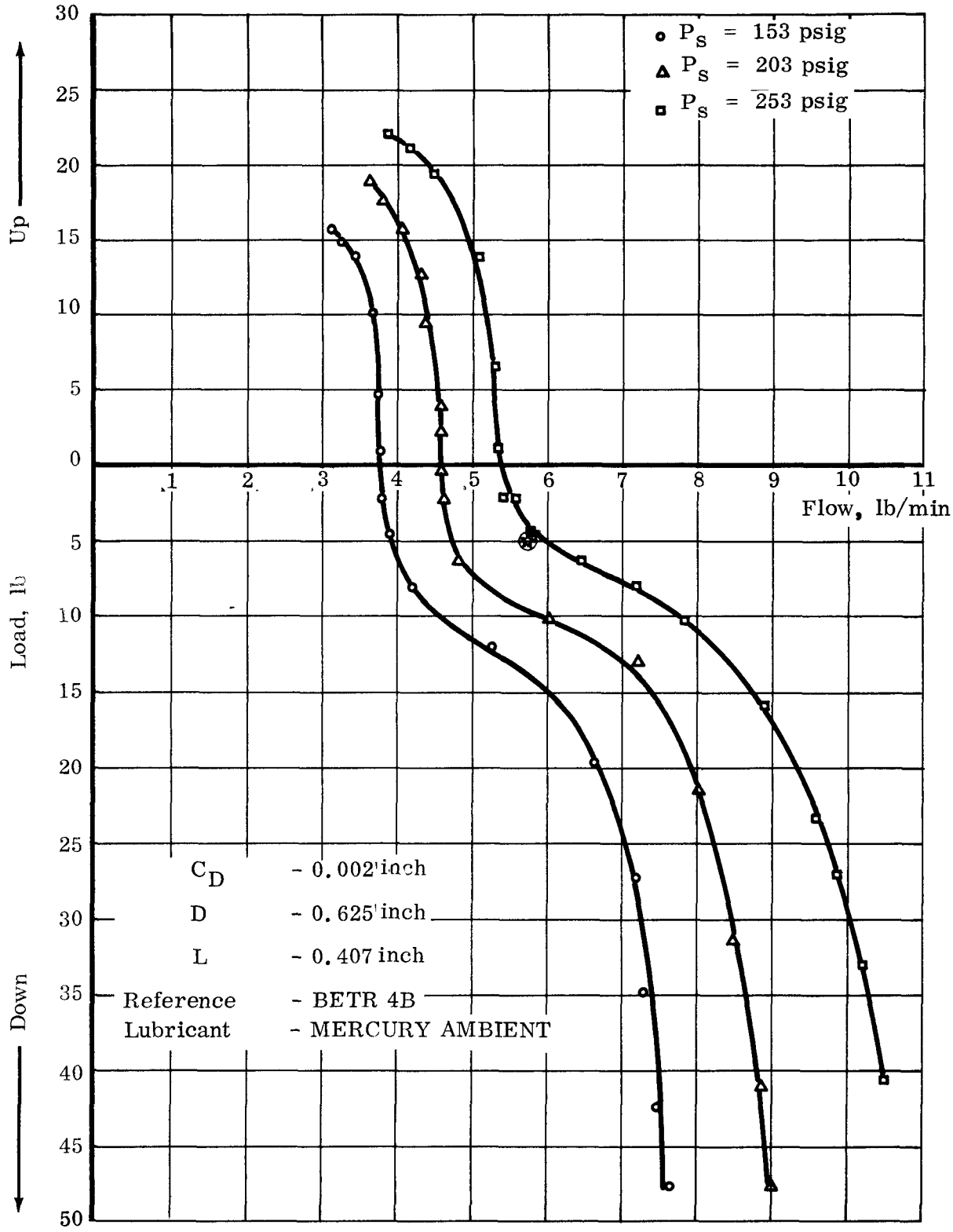

Figure 30. Load vs Flow for a Plain Bearing with a Single Inlet at the Top at 20,000 rpm

Most significant was the absence of half-frequency whirl at any flow or load conditions from zero to maximum speed of 30, 000 rpm. This reversed the trend from the balanced rotor to the 30 lb unbalance. As indicated in Figure 8, the 30 lb unbalanced rotor resulted in a less stable bearing than the balanced rotor. These data, therefore, agree with experience that an unbalanced rotor, when the unbalance is great enough, has better stability characteristics than a balanced rotor. However, these three tests demonstrate that there is an optimum magnitude of unbalance for stability for the plain journal bearing lubricated with mercury. The penalty paid for stability is a large synchronous component which can get large enough to exceed the capacity of the bearing when unidirectional load is added. This is in fact what happened at 30, 000 rpm in BETR 4B.

The increase in synchronous whirl amplitude with speed can be seen from Figure 31, which is a composite of the photographed locus as speed was increased. The initial speed of 1, 000 rpm indicated a run out of some 0.0002 inch (diameter). At 24, 000 rpm the synchronous whirl amplitude at the point of measurements (some 2 inches from the center of the alternator end bearing) was equivalent to the bearing clearance. An additional 0.0003 inch (diameter) increase in amplitude occurred in reaching 30, 000 rpm. The total shaft deflection at 30, 000 rpm then represents a combination of some shaft bending (a minimum of 0.0003 inch diameter) and synchronous whirl of the shaft in the bearing (a maximum of 0.002 inch). Figure 32 shows a series of the shaft deflection locus photographs from 1, 000 to 30, 000 rpm. No half-frequency whirl is present.

Additional load and flow-pressure data for different hydrodynamic bearings may be found in Table 1 which is taken from Reference 1.

H. DAMPING CHARACTERISTICS

Mercury-lubricated, turbulent-flow bearings have damping coefficients that approach the critically damped conditions. Figure 33 shows a useful method of establishing critical speed and damping characteristics. For the plain bearing, the first mode bearing-rotor critical was encountered near 7500 rpm (corresponding to a phase shift of approximately 90°). However, an approximately 180° phase change required a frequency band from 1, 000 to 25, 000 rpm. This, plus the very small increase in shaft amplitude, is an indication of damping in the fluid film. In this case, the plain bearing was approximately one-half critically damped ($C/C_{cr} \approx 0.5$). This characteristic is extremely advantageous where critical speed and half-frequency whirl are concerned. Shaft displacement in the bearing is difficult to detect or small on passing through a critical, thus permitting operation at or close to bearing-rotor critical speeds without disasterous effects, even though it is not advisable for extended periods. Because damping characteristics are high, operation with half-frequency whirl present is permissible without serious results. Once the threshold of instability is reached, it is possible to increase speed and rely upon the damping characteristics and the squeeze film action to continue carrying load. However, as indicated in Figures 15 and 16, the whirl amplitude increases rapidly, and operation continues at dangerously small film thicknesses.

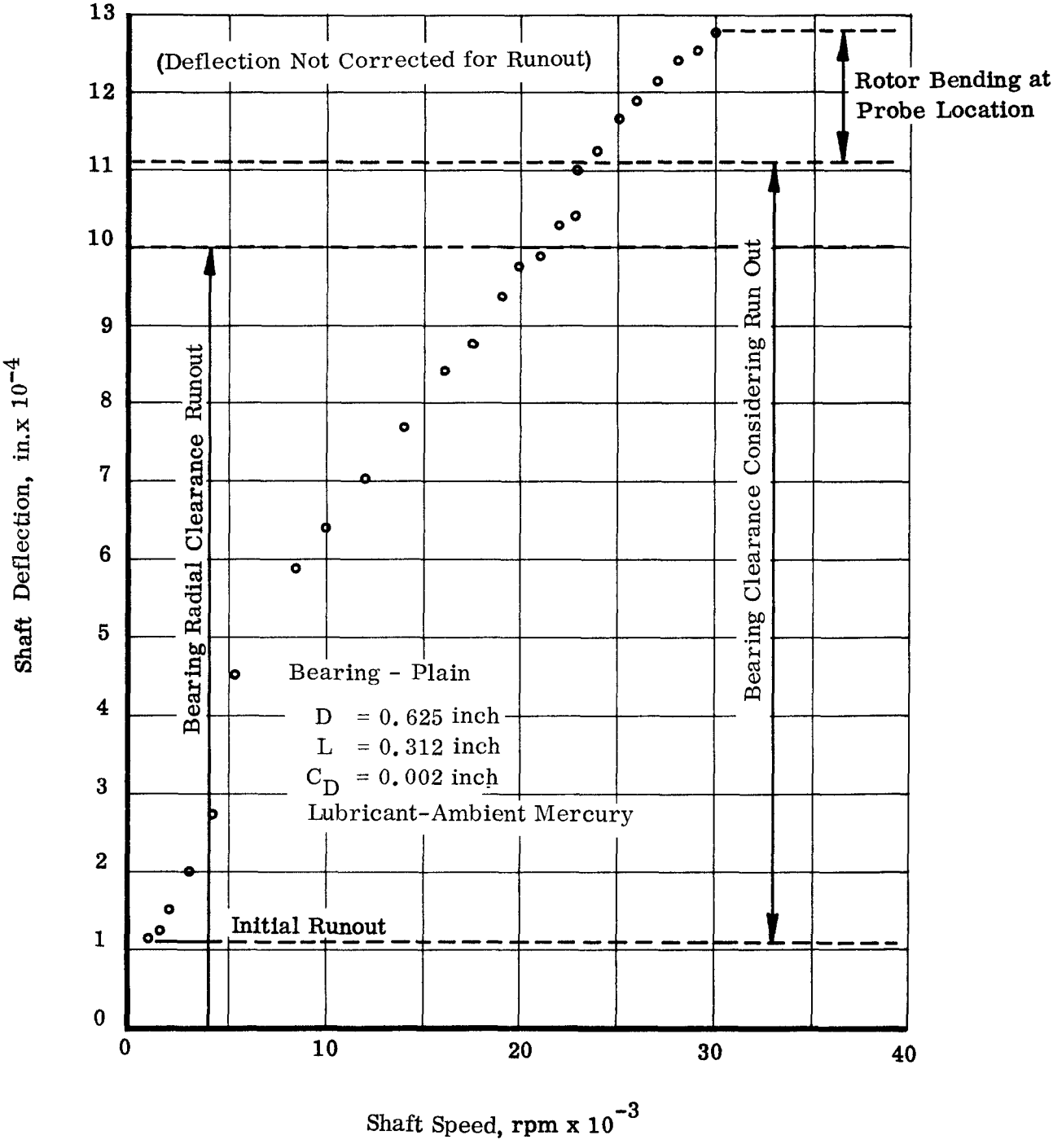

Figure 31. Shaft Deflection vs Shaft Speed
Test BETR 4B

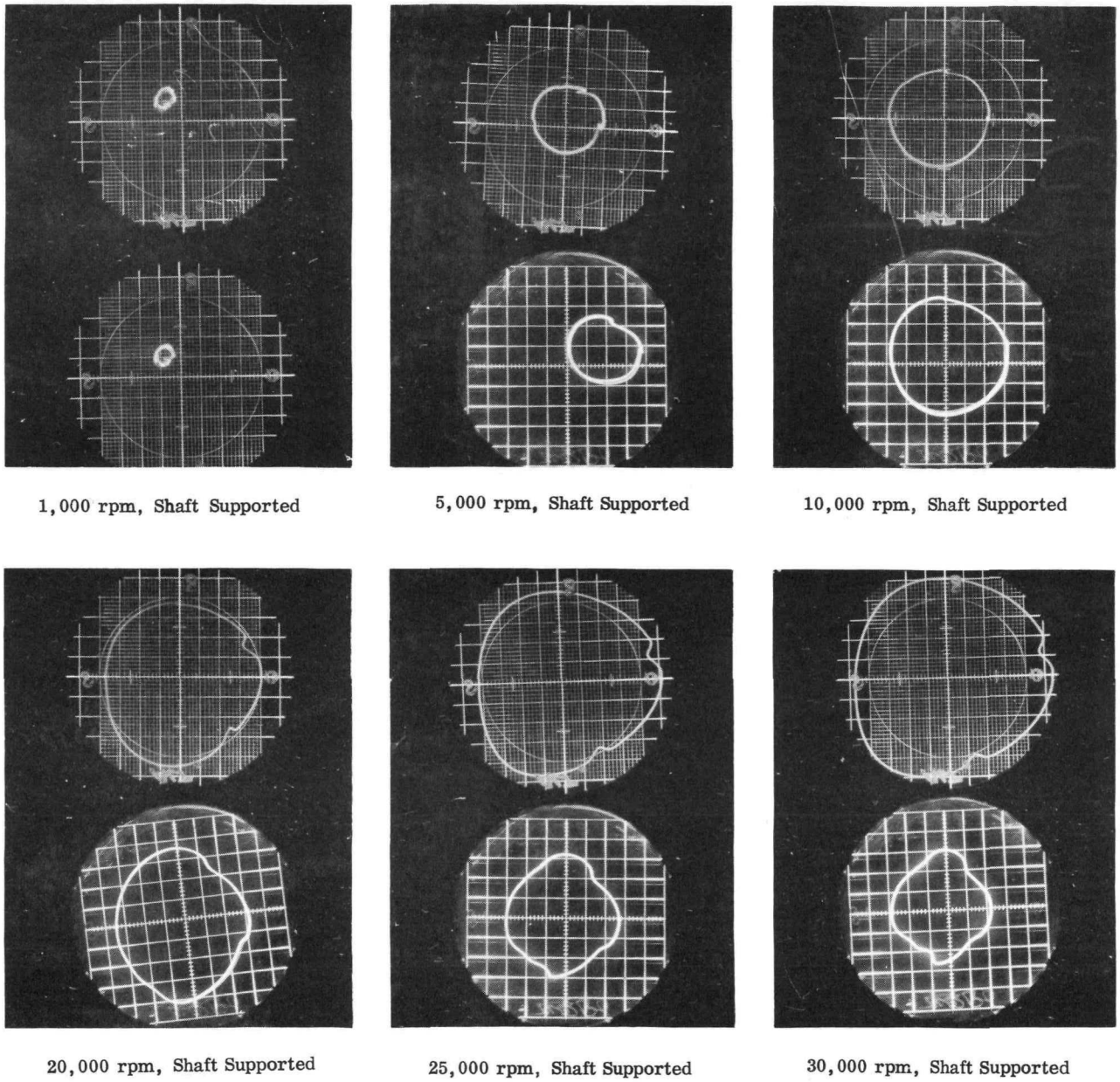

1,000 rpm, Shaft Supported

5,000 rpm, Shaft Supported

10,000 rpm, Shaft Supported

20,000 rpm, Shaft Supported

25,000 rpm, Shaft Supported

30,000 rpm, Shaft Supported

Figure 32. Synchronous Whirl Amplitude as a Function of Speed
BETR 4B Test Series

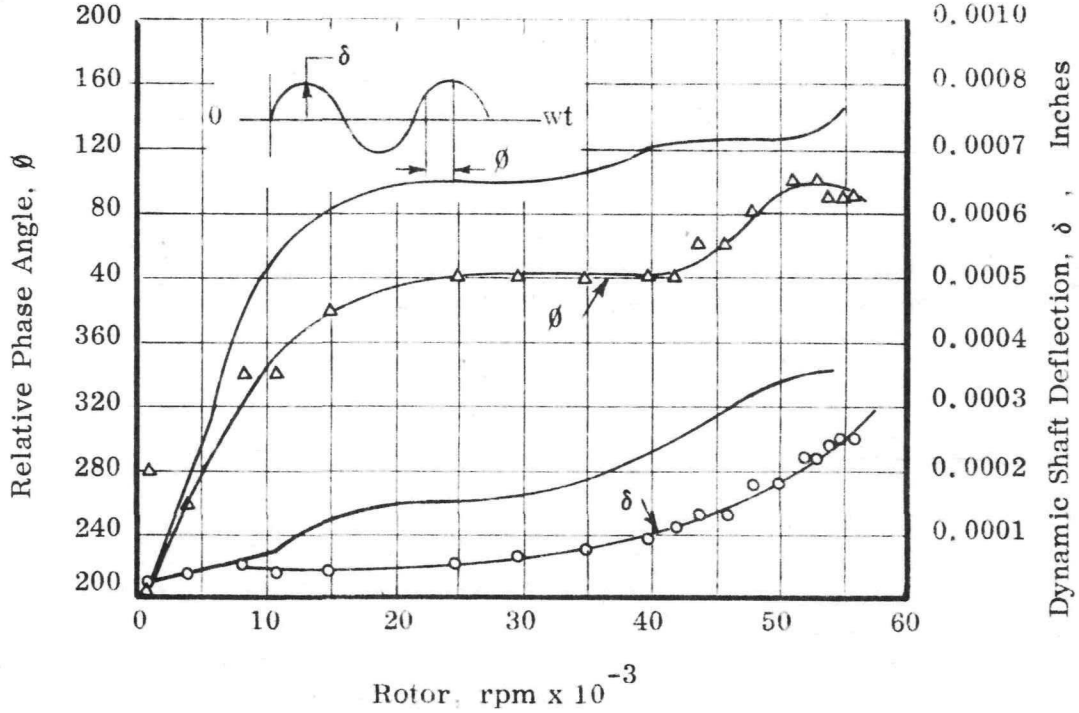

Figure 33. Relative Phase Angle and Dynamic Deflection vs Rotor Speed

TABLE 1

PERFORMANCE SUMMARY FOR FIVE JOURNAL BEARINGS

Lubricant	Hole	Axial Groove	Tangential Inlet Groove	Annular	Load Pad
Lube Supply Temperature, °F	75	75-400	75-400	75	75
Operating Speed, rpm	10,000	40,000	40,000	40,000	40,000
Power Consumption, watts	------	180-220	180-220	180-220	180-220
Diametral Clearances Tested, Inches	0.0010	0.0010, 0.0012 0.0014, 0.0020	0.0012, 0.0014 0.0020	0.0010, 0.0013 0.0015	0.0010, 0.0005
Average Lube flow At 2.5 pounds Applied Radial Load, lb/min	1.0 at 300 psig	2.0 at 150 psig (C_D = 0.0020)	1.1 at 150 psig (C_D = 0.0014)	3.0 at 150 psig (C_D = 0.0015)	2.6 at 100 psig (C_D = 0.0010)
Average Lube Flow at 25 pound applied Radial Load, lb/min	------	7.4 at 150 psig (C_D = 0.0020)	3.6 at 150 psig (C_D = 0.0014)	4.2 at 150 psig (C_D = 0.0005)	3.8 at 150 psig (C_D = 0.0010)
Maximum Load Tested, lb	2.5	25	25	35	25

The influence of rotating load (30 lb/bearing at 40,000 rpm) on phase angle and dynamic shaft deflection is shown in Figure 34, and compared to the balanced case in Figure 33. The shape of phase angle and deflection curves, as a function of frequency, remain unchanged. The deflection is, of necessity, greater because of the unbalance. The phase angle zero setting appears to have been displaced some 40° to 60°, but this was probably due to the out-of-phase relationship between the unbalance vector and the run-out of the shaft at the point where phase angles are measured. Comparing the balanced and unbalanced cases in Figure 33 indicates that unbalance does not influence the degree of damping present in the bearing. However, because of the high damping characteristic, it is difficult to conclude the influence of rotating load on the frequency of the first mode rotor-bearing critical speed because of the small deflections measured. But based on phase angle, no change appears to have occurred in the frequency at which the first mode critical was encountered in the unbalanced case. Squeeze film action also appears greater because of the high inertia of the mercury fluids.

I. FILM CONTINUITY

The use of mercury as the lubricant creates a problem in the clearance space because two-phase flow (liquid and vapor) exists. End leakage, high and low pressure regions, and high temperatures cause vapor bubbles to form in the unloaded portion of the bearing. If allowed to collapse in the bearing clearance space these bubbles will cause cavitation-erosion damage. This type of damage is greatest in bearings that generate hydrodynamic pressures and have high supply pressure, i. e., three pad and plain types mostly. If the vapor bubbles pass from the bearing without collapsing via slots or grooves referenced to drain pressures, as in the three-sector type, damage caused by this phenomenon is eliminated or reduced to permit reliable long-term operation.

An additional problem created by two-phase flow in the clearance space is reduction in load capacity, if the vapor is carried into the loaded portion of the bearing, or if loads are rotating.

III. CONCLUSIONS

The plain bearing as developed in the BETR 4 test series met many of the imposed CRU requirements. It was applied in the CRU I, III and IV M alternator modules with varying success. The longest run in the CRU I series was 483 hours. In the CRU III module the longest run was 588 hours. In CRU IV-M 435 hours were achieved which far exceeded the initial requirement of 200 hours at design point. Nevertheless, the plain journal bearing had certain disadvantages which prevented it from being considered for application in the final CRU version that required a 10,000 hour (one year) life. These disadvantages were:

1) Poor stability characteristics: Half-frequency whirl was encountered at very low speeds

2) Poor predicted life capability because of sensitivity to cavitation-erosion type damage

3) Unreliable flow characteristics under the influence of large rotating loads or unidirectional loads into the supply pad

4) Very sensitive to clearance change

5) High supply pressure requirement to force adequate coolant flow through the bearing.

The following significant conclusions were possible as a result of the component development activity:

1) The technique of using the Smith and Fuller turbulent end leakage correction for hydrodynamic load capacity agreed reasonably well with experimental results.

2) The turbulent or superlaminar performance characteristics of a plain journal bearing could be predicted by applying a Reynolds number correction factor to the laminar flow load capacity equation as follows:

$$W_T = W_c \; 0.0301 \, (R_{eho})^{0.553}, \text{ where } 1000 < R_{eho} < 6000$$

3) The measured attitude-eccentricity locus data was in good agreement with that measured by Smith and Fuller and indicated a considerable increase in attitude angle for a given eccentricity ratio over the laminar case.

4) The measured power loss agreed well with the semi-empirical equation defined by Smith and Fuller as

$$H_T = H_{Petroff}^{x} \quad 0.039\ (R_e)^{0.57}$$

5) Load required to suppress onset of half frequency whirl instability was predicted accurately by the method utilized during this development program.

6) Measured flow-pressure characteristics did not agree with prediction. However, semi-empirical equations were developed which can be used to predict flow characteristics as follows:

At zero speed, $Q_o = 0.475\ (P_S)^{0.65}$, lb/min

At speed N, $Q_N = 357\ N^{-1.24}\ P_s^{1.5}$, lb/min

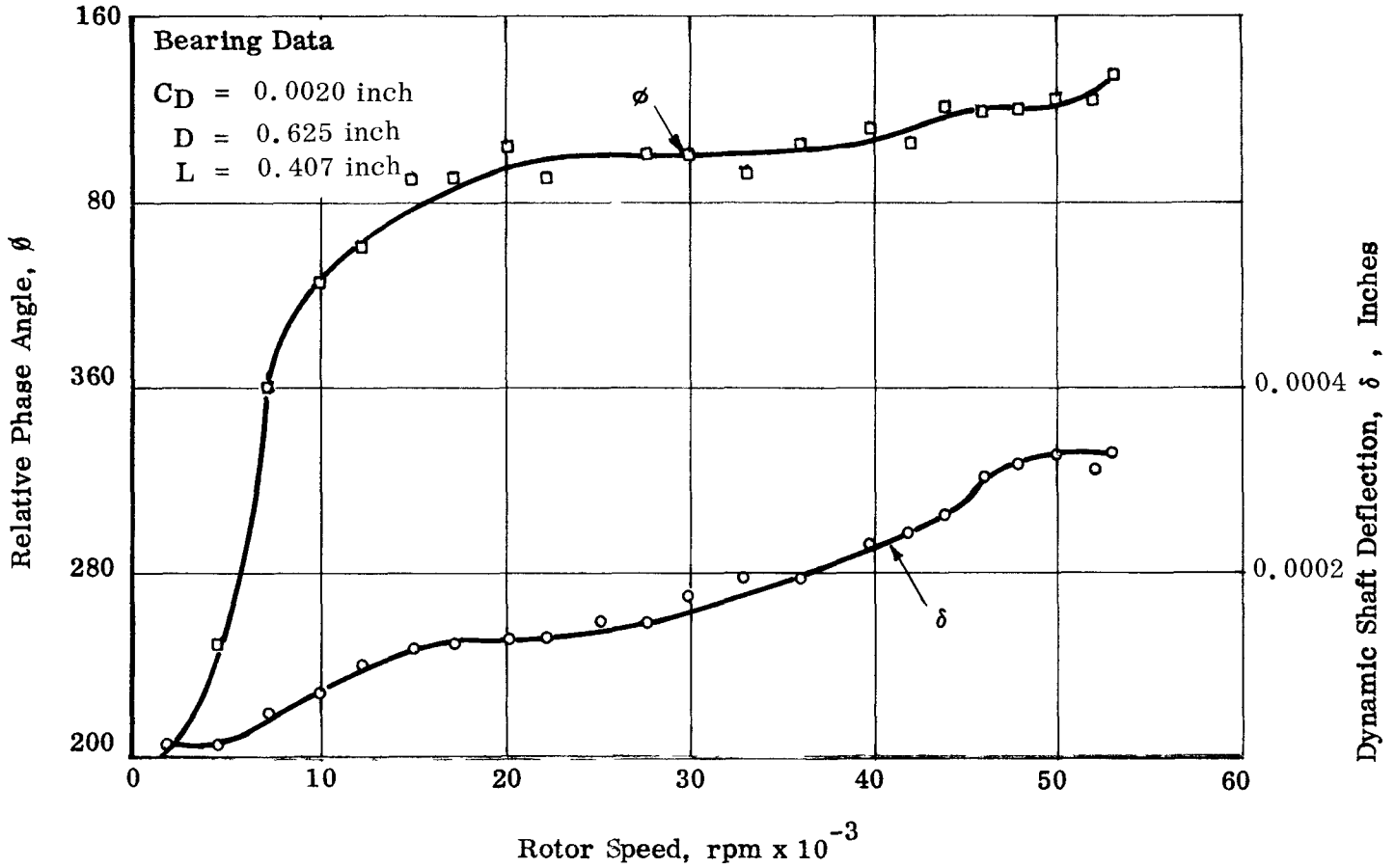

Figure 34. Relative Phase Angle and Dynamic Shaft Deflection vs Rotor Speed
(Experimental Test No. BETR 4A for 30 lb/brg Unbalance at 40, 000 rpm)